



HAL
open science

Anticyclonic and cyclonic eddies of subtropical origin in the subantarctic zone south of Africa

Michel Arhan, Sabrina Speich, Christophe Messenger, Guillaume Dencausse, Rana Fine, Marie Boye

► **To cite this version:**

Michel Arhan, Sabrina Speich, Christophe Messenger, Guillaume Dencausse, Rana Fine, et al.. Anticyclonic and cyclonic eddies of subtropical origin in the subantarctic zone south of Africa. *Journal of Geophysical Research*, 2011, 116, pp.C11004. 10.1029/2011JC007140 . hal-00669706

HAL Id: hal-00669706

<https://hal.science/hal-00669706>

Submitted on 13 May 2012

HAL is a multi-disciplinary open access archive for the deposit and dissemination of scientific research documents, whether they are published or not. The documents may come from teaching and research institutions in France or abroad, or from public or private research centers.

L'archive ouverte pluridisciplinaire **HAL**, est destinée au dépôt et à la diffusion de documents scientifiques de niveau recherche, publiés ou non, émanant des établissements d'enseignement et de recherche français ou étrangers, des laboratoires publics ou privés.

Anticyclonic and cyclonic eddies of subtropical origin in the subantarctic zone south of Africa

Michel Arhan,¹ Sabrina Speich,² Christophe Messenger,¹ Guillaume Dencausse,^{1,3} Rana Fine,⁴ and Marie Boye⁵

Received 16 March 2011; revised 12 July 2011; accepted 27 July 2011; published 3 November 2011.

[1] Two eddies, one anticyclonic and the other cyclonic, intersected in the Subantarctic Zone south of South Africa during a hydrographic transect, are described using a large set of measurements including full depth hydrography, Acoustic Doppler Current Profiler velocities, biogeochemical tracers, air-sea fluxes and altimetric sea surface height. Both eddies have a subtropical origin. The anticyclone is an Agulhas ring with convected core water of $\sim 12^{\circ}\text{C}$, and swirl velocities of 1 m s^{-1} . It was 9.5 months old when sampled and had crossed the Agulhas Ridge. Though sampled in summer, it was releasing $\sim 200\text{ W m}^{-2}$ (sensible plus latent heat flux) to the atmosphere. It was observed adjacent to the Subantarctic Front, illustrating the usual encounters of such structures with this front. The cyclone, marked by pronounced low oxygen and CFC anomalies revealing an origin at the continental slope, was 4.5 months old. It had swirl speeds of 0.3 m s^{-1} , and was coupled with the anticyclone when observed. From their kinematics and water mass properties both structures were found to transport subtropical water down to $\sim 900\text{ m}$, the water trapped below this depth being either from the northern Subantarctic Zone, or local water. The two structures illustrate the capacity of eddies in the region to transfer subtropical and alongslope water properties into the Subantarctic Zone.

Citation: Arhan, M., S. Speich, C. Messenger, G. Dencausse, R. Fine, and M. Boye (2011), Anticyclonic and cyclonic eddies of subtropical origin in the subantarctic zone south of Africa, *J. Geophys. Res.*, 116, C11004, doi:10.1029/2011JC007140.

1. Introduction

[2] *Lutjeharms* [1988] first suggested that the meridional propagation of mesoscale eddies at distinct sectors of the Subtropical Front (STF), such as those bordering the western boundary currents, might be an important process for the transport of heat into the Southern Ocean. The oceanic domain south of South Africa, where the Agulhas Current system abuts on the Antarctic Circumpolar Current (ACC), should naturally be counted among such sectors. In agreement with this view, *Dencausse et al.* [2011] recently observed that, due to the intense mesoscale activity of that region [e.g., *Boebel et al.*, 2003], the STF, which is present at 38°S – 42°S in the eastern South Atlantic and western South Indian oceans, is interrupted between about 12°E and 23°E .

[3] This ~ 10 -degree longitudinal interval appears as a preferential pathway for mesoscale structures. Here, indeed,

warm eddies of subtropical origin have sometimes been observed to enter the Subantarctic Zone (SAZ) located between the STF and the Subantarctic Front (SAF) of the ACC [*Lutjeharms and Valentine*, 1988; *Arhan et al.*, 1999; *Gladyshev et al.*, 2008]. Most of these observed mesoscale features have been anticyclones, either *Agulhas eddies* shed southward by the meandering Agulhas Return Current, or *Agulhas rings* formed at the Agulhas Current retroflection. However, as anticyclones tend to propagate equatorward under the β -effect, Agulhas rings that enter the SAZ (located poleward of their formation region) are not numerous. *Dencausse et al.* [2010] observed that these structures (about 2 per year) often result from subdivisions of newly spawned rings at the northeastern tip of the Agulhas Ridge (Figure 1).

[4] On the other hand, owing to the β -effect, which tends to drive them poleward, the cyclones of subtropical origin present in the southeastern Cape Basin and in the Agulhas Basin (Figure 1) should be more prone to enter the SAZ. *Boebel et al.* [2003] and *Lutjeharms et al.* [2003] showed that these structures can fall into two categories, namely, Cape Basin cyclones, formed along the western coast of South Africa, and Agulhas cyclones formed inshore of the Agulhas Current. Tracking them from altimetric Sea Surface Height data and surface/subsurface float displacements, *Boebel et al.* [2003], *Morrow et al.* [2004], *Richardson* [2007], *Rubio et al.* [2009], and *Baker-Yeboah et al.* [2010a, 2010b] all found trajectories orientated southwestward, and clearly contrasting with the dominant northwestward

¹Laboratoire de Physique des Océans, UMR6523, CNRS/Ifremer/IRD/UBO, Ifremer/Centre de Brest, Plouzané, France.

²Laboratoire de Physique des Océans, UMR6523, CNRS/Ifremer/IRD/UBO, UBO-UFR Sciences et Techniques, Brest, France.

³Now at LEGOS/OMP, Toulouse, France.

⁴RSMAS/MAC, University of Miami, Miami, Florida, USA.

⁵Laboratoire des Sciences de l'Environnement Marin, UMR6539, CNRS/IRD/UBO, IUEM, Technopole Brest Iroise, Plouzané, France.

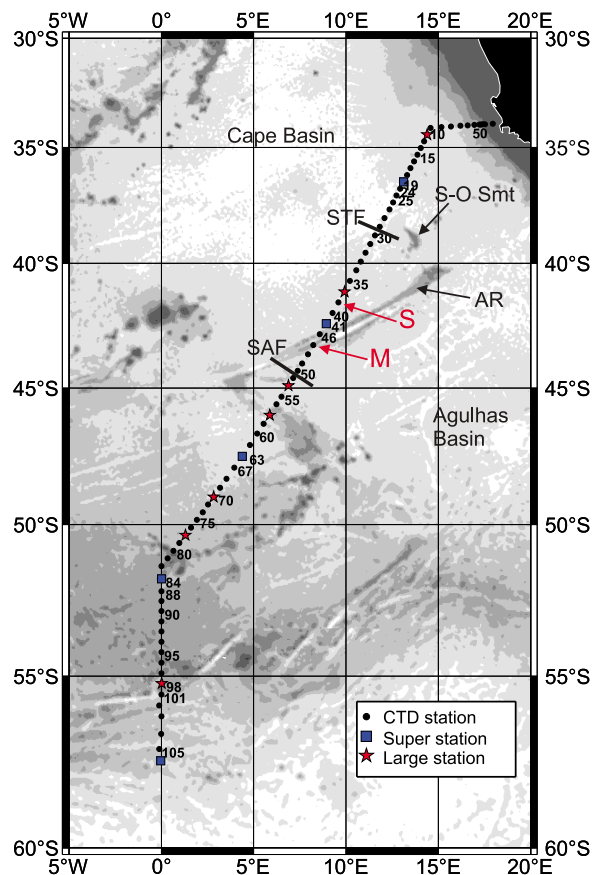


Figure 1. Map of the GoodHope/BGH hydrographic line, with the locations of eddies S (station 39) and M (station 47). Also shown are the locations of the Subtropical Front (STF) and Subantarctic Front (SAF) based on criteria defined by Orsi *et al.* [1995]. Only the northern branch of the STF is shown (see text). AR and S-O Smt stand for Agulhas Ridge and Schmitt-Ott Seamount, respectively. Stars and squares show the multicast stations.

orientation of Agulhas rings routes. The cyclones were found to be more numerous than the anticyclones in the region, yet with a shorter average life-time of 2–3 months [Boebel *et al.*, 2003] and a limited number of trajectories extending southward beyond 40°S, in the SAZ. Weaker initial dynamic characteristics (e.g., azimuthal velocities) of the cyclones, as compared with the anticyclones, might be a cause for their shorter life-time and trajectories. Richardson [2007] observed that the trajectories of numerous Agulhas cyclones stop near the northeastern end of the Agulhas Ridge and neighboring seamounts (~40°S–15°E), that is, just north of the SAZ northern boundary.

[5] The international GoodHope program was undertaken in 2004 to monitor the exchange of water and properties between the Atlantic and Indian oceans, and to better understand the processes involved in these exchanges. As one part of the program, repeat hydrographic samplings of a quasi-meridional line (hereafter the GoodHope line; Figure 1) provide estimates of the zonal volume transports south of Africa. While such large scale analyses are being pursued [Gladyshev *et al.*, 2008; Swart *et al.*, 2008], the

repeat sections are also useful with regard to the mesoscale features which they happen to intersect. Gladyshev *et al.* [2008] discussed the behavior and properties of one of the above mentioned Agulhas rings which, after spending a few months in the SAZ, returned to the subtropical domain where it was sampled during the 2004 cruise. Swart and Speich [2010], inferring the heat content variability along the GoodHope line from Sea Surface Height data, found that structures of this kind dominate the variability in the SAZ. In this article, we describe two subtropical eddies that were observed in the SAZ during the 2008 GoodHope cruise. One eddy, anticyclonic and adjacent to the SAF when observed, is an Agulhas ring with a thick (~500 m) homogeneous core. The other eddy, found north of the former and apparently coupled to it when observed, is cyclonic with core water properties suggestive of an origin near the African continental slope.

[6] A large number of measurements, including hydrography, tracers, Vessel-Mounted and Lowered Acoustic Doppler Current Profiles (VM-ADCP, L-ADCP), and air-sea fluxes, were realized during the 2008 GoodHope cruise. These measurements, complemented by altimetric Sea Surface Height (SSH) data, provide detailed descriptions of the properties and histories of the two eddies. After presenting the GoodHope 2008 data and first eddy evidence in section 2, we discuss the properties and behavior of the anticyclone (hereafter referred to as eddy M) in section 3, and of the cyclone (eddy S) in section 4. Section 5 gives a summary of the results along with some concluding remarks.

2. The 2008 GoodHope Data and Eddies M and S in Their Large Scale Environment

[7] The 2008 cruise of the GoodHope program was carried out in the framework of the International Polar Year, and was named the BONUS-GoodHope cruise (hereafter BGH), as it associated the fourth hydrographic sampling of the GoodHope line with biogeochemical measurements constitutive of the BONUS program. The BGH measurements were carried out from the French R/V *Marion Dufresne* between 7 February and 24 March 2008, from Cape Town to Durban. A total of 111 hydrographic profiles were obtained at 79 geographical stations, from the African continental slope (33°59'S–17°14'E) to beyond the ACC Southern Boundary along the Greenwich meridian (57°33'S, 0°E). In the following the on-station data are referred to using the hydrographic profile numbers. Further information on the cruise and the groups in charge of the various measurements may be found in the cruise report [Speich and Dehairs, 2008], and details of the hydrographic measurements in the Conductivity-Temperature-Depth (CTD) data report [Branellec *et al.*, 2010]. In addition to hydrographic measurements, we here use the chlorofluorocarbon (CFC-11 and CFC-12) measurements [e.g., Fine *et al.*, 1988; Fine, 2011], the nutrient data, and the VM-ADCP data to characterize the two eddies. Two ARGO profilers from the French Coriolis program were launched in the eddies, and weekly fields of absolute SSH were used to get the eddy trajectories. These SSH data were obtained from the Archiving, Validation and Interpretation of Satellite Oceanographic database (AVISO), produced by Ssalto/Duacs with support from the French Centre National d'Etudes Spatiales (<http://www.aviso.oceanobs.com>).

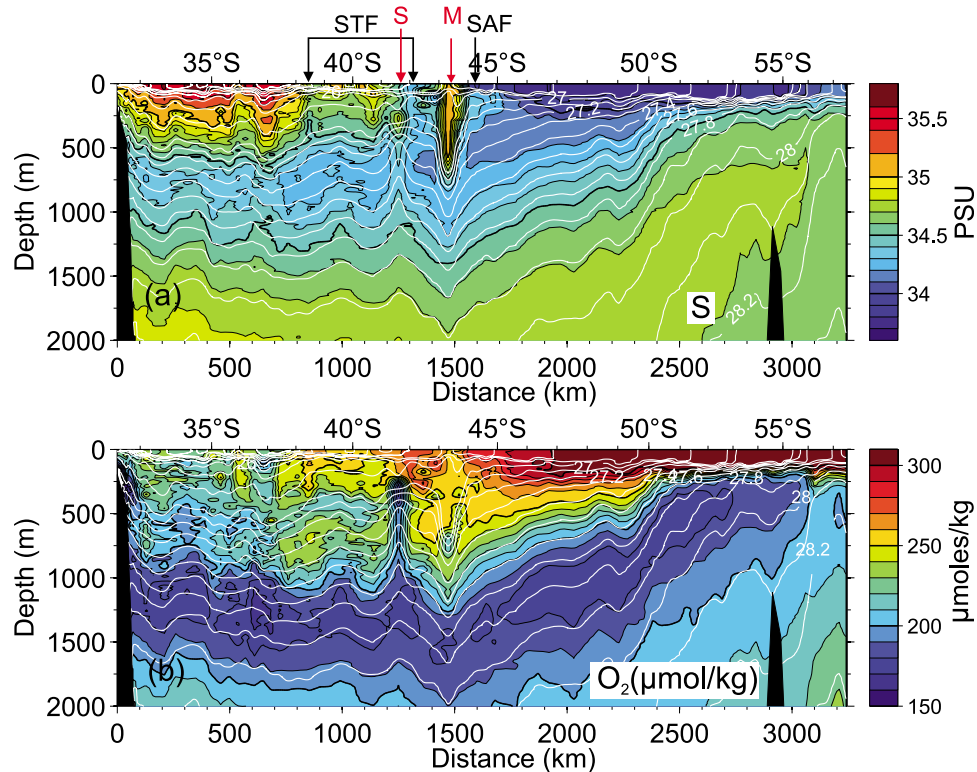


Figure 2. (a) Salinity and (b) dissolved oxygen along the BGH line. The locations of the two eddies (M, S) and of the STF (two branches) and SAF are indicated. The superimposed isopycnals are neutral density isopycnals.

[8] Eddies M and S stand out in the salinity and dissolved oxygen vertical distributions along the GoodHope line, as a pronounced salinity maximum at $43^{\circ}20'S-8^{\circ}14'E$ and depths 0–600 m for M, and as an oxygen minimum at $41^{\circ}36'S-9^{\circ}35'E$ and depths 300–1000 m for S (Figure 2). Associated with these signatures are vertical excursions of the isopycnals, bowl-shaped for M and doming for S, detected as deep as 2000–2200 m for both structures. The locations of the STF and Subantarctic Front (SAF), also shown in Figure 2, are based on the hydrographic criteria proposed by Orsi *et al.* [1995]. The SAF criterion positioned the front in the relatively narrow latitude interval $44^{\circ}S-45^{\circ}S$, just south of eddy M. The STF criteria (potential temperature change from $10^{\circ}C$ to $12^{\circ}C$, and salinity change from 34.6 to 35.0, at 100 m), however, led to a wide latitudinal span for this front, from $38^{\circ}20'S$ to $42^{\circ}S$, suggestive of two branches at these latitudes. The northern limit of this interval shows the most pronounced gradient (e.g., salinity change from 34.7 to 35.0, at 100 m), and lies at the southern border of the wide saline domain ($S > 35.0$) marking the subtropical waters south of Africa. The southern limit of the STF detection interval coincides with the southern border of eddy S (Figure 2a).

[9] The SSH AVISO map for the period of sampling (Figure 3) shows the SAF and the northern branch of the STF. The latter is here located at the southern border of a SSH ridge connecting two Agulhas rings. The southern branch of the STF is not visible in the SSH distribution. An elongated southward meander of this front does exist east of

the two eddies and north of S along the BGH track, but this meander does not encompass the SSH signature of eddy S which, likely owing to its low anomaly, is rather connected to the SAF.

[10] The two eddies also stand out in the distributions of the VM-ADCP velocities along the track of the BGH cruise (Figure 4). Eddy M is particularly visible right above the Agulhas Ridge, through swirl velocities as high as 1 m s^{-1} (displayed velocities are averaged over 5 km distances, and in layer 100–400 m). North of it, eddy S has maximum velocities around 0.3 m s^{-1} . In both structures, the nearly parallel directions of the opposite velocity vectors associated with the eddy rotational motions indicate that the cruise track intersected the structures close to their centers. By superimposing the frontal locations on Figure 4, we observe that the Polar Front, the SAF, and the northern branch of the STF all correspond to velocities with an eastward component. In contrast, the southern branch of the STF, being located at the southern border of eddy S (at $42^{\circ}S$), is associated with velocities with a westward component.

[11] Referring to the work of Dencausse *et al.* [2011] on the STF discontinuity in this region, the location where the northern branch of the STF was found during BGH ($38^{\circ}20'S-12^{\circ}E$) is about the easternmost point where this front could be detected from its SSH signature at the time of sampling (Figure 3). Farther east, the front becomes entangled in intense mesoscale structures. The observation of this branch at about $38^{\circ}S$, the approximate latitude where the STF is usually observed in the eastern South

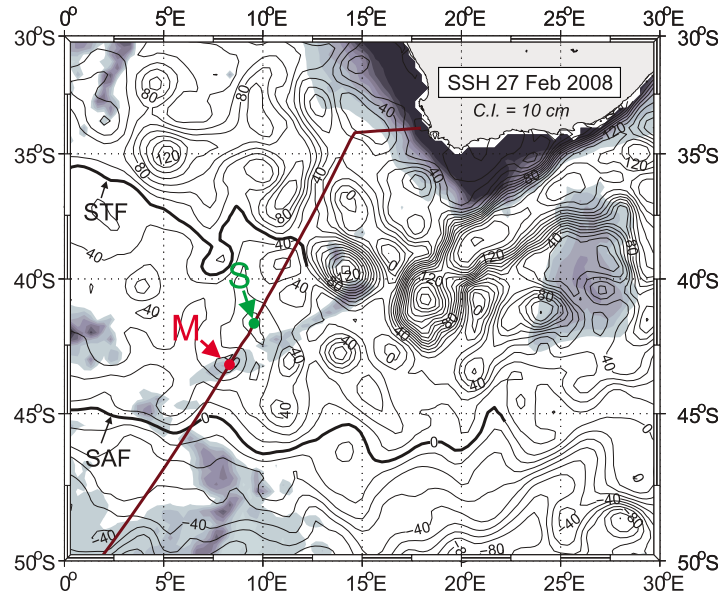


Figure 3. AVISO SSH map on 27 February 2008. Superimposed are the locations of eddies M (red; observed on 28 February) and S (green; observed on 26 February).

Atlantic [e.g., Stramma and Peterson, 1990], gives confidence that the northern STF branch observed during BGH is the eastern end of the classical South Atlantic STF (or southern STF of Belkin and Gordon [1996]). From

Figures 2a and 3, on the other hand, what we named the southern branch looks more like a local elongated meander of diluted subtropical water. It seems therefore justified to consider that the SAZ spans latitudes from 38°20'S to 44°S

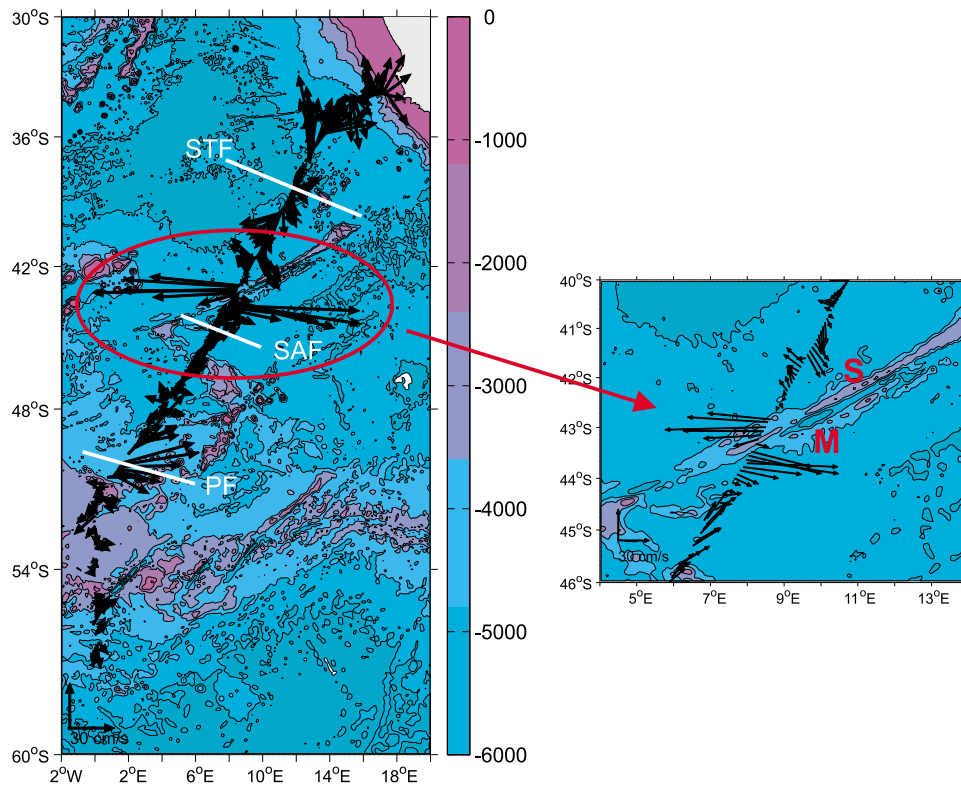


Figure 4. VM-ADCP velocities in layer 100–400 m along the whole BGH line and in the region of eddies M and S, processed following Izenic et al. [2005]. Velocities are averaged over 5 km distances. Colors and black contours represent bathymetry. The contour interval is of 1000 m. The positions of the major Southern Ocean fronts at the dates of the cruise are superimposed in white.

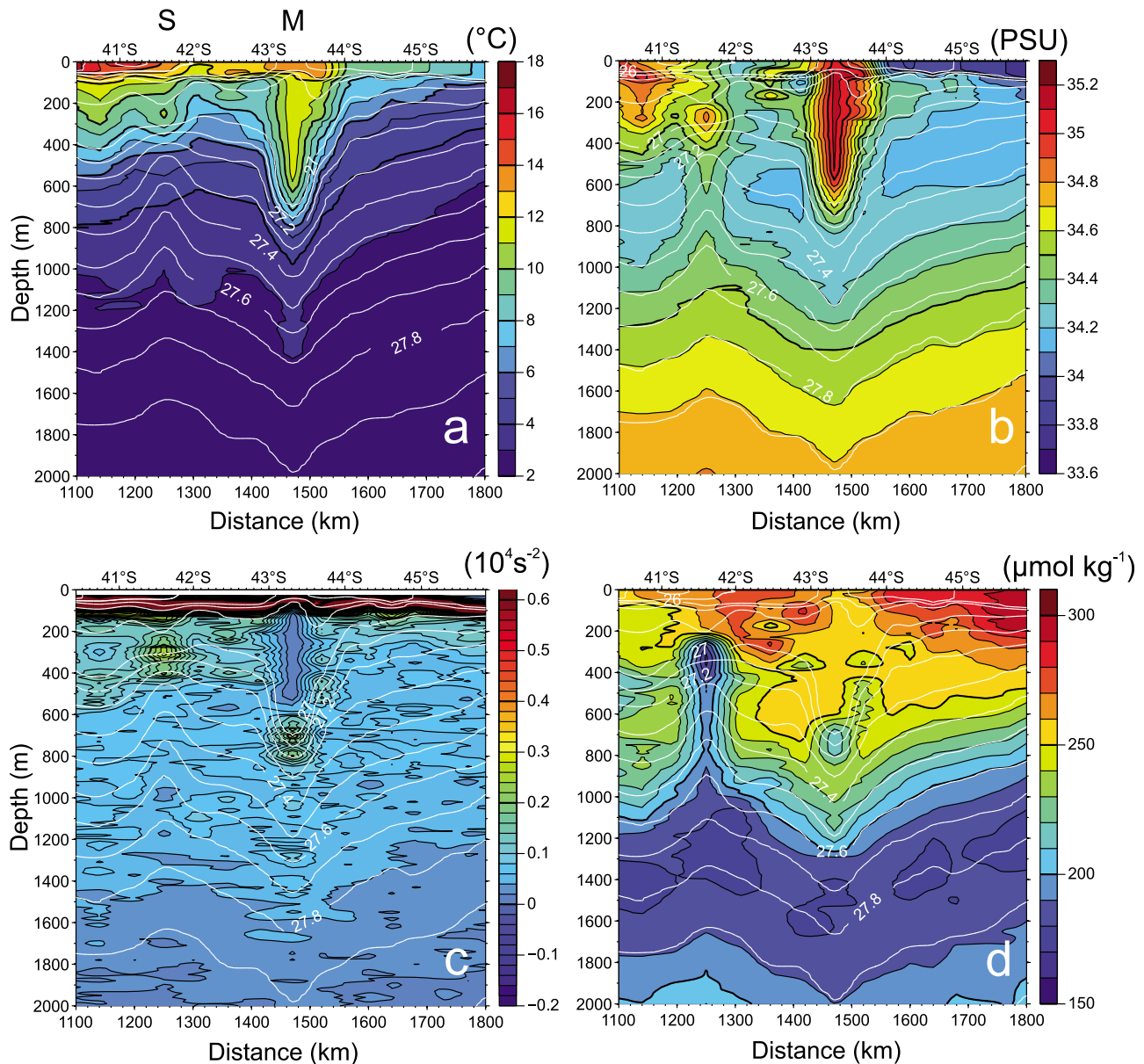


Figure 5. Vertical distributions of (a) potential temperature, (b) salinity, (c) squared Brunt-Väisälä frequency and (d) dissolved oxygen concentration across eddies M and S. Superimposed are the neutral density isopycnals.

along the cruise track, to regard the waters of intermediate properties between $38^{\circ}20'S$ and $42^{\circ}S$ as just a local southward protrusion, and to view eddy S as located in the SAZ.

3. Anticyclone M

3.1. Core Properties and Origin of Eddy M

[12] The following description of the core properties of eddy M rests on expanded views of vertical property distributions in the region of the two eddies and at depths 0–2000 m. They show the potential temperature (θ), salinity, squared Brunt-Väisälä frequency and dissolved oxygen in Figure 5, and CFC-11, CFC-12, nitrate and silicate in Figure 6. Although the rotational velocity signature of eddy M was sampled at 3 hydrographic stations (stations 46, 47,

48, see section 3.3), the eddy core properties were only observed at station 47. In order to better contrast the core properties with those of surrounding waters, Figure 7 displays the salinity and oxygen profiles, and the neutral density (γ)-salinity and neutral density-dissolved oxygen curves at this eddy core station and at the adjacent stations.

[13] The core of eddy M is characterized by a 500 m-thick homogeneous layer, between ~ 80 m and ~ 580 m, itself capped by a 30 m surface mixed layer and the intervening pycnocline (Figures 5 and 7). The homogeneous layer has properties $\theta = 11.8^{\circ}C$, $S = 35.15$, $O_2 = 257.7 \mu\text{mol kg}^{-1}$, and $\gamma = 26.82 \text{ kg m}^{-3}$ ($\sigma_0 = 26.75 \text{ kg m}^{-3}$). With a core temperature lower than $12^{\circ}C$, M is among the coldest of comparable eddies sampled in the region, very similar to Agulhas ring R1 reported by Arhan *et al.* [1999] (Table 1),

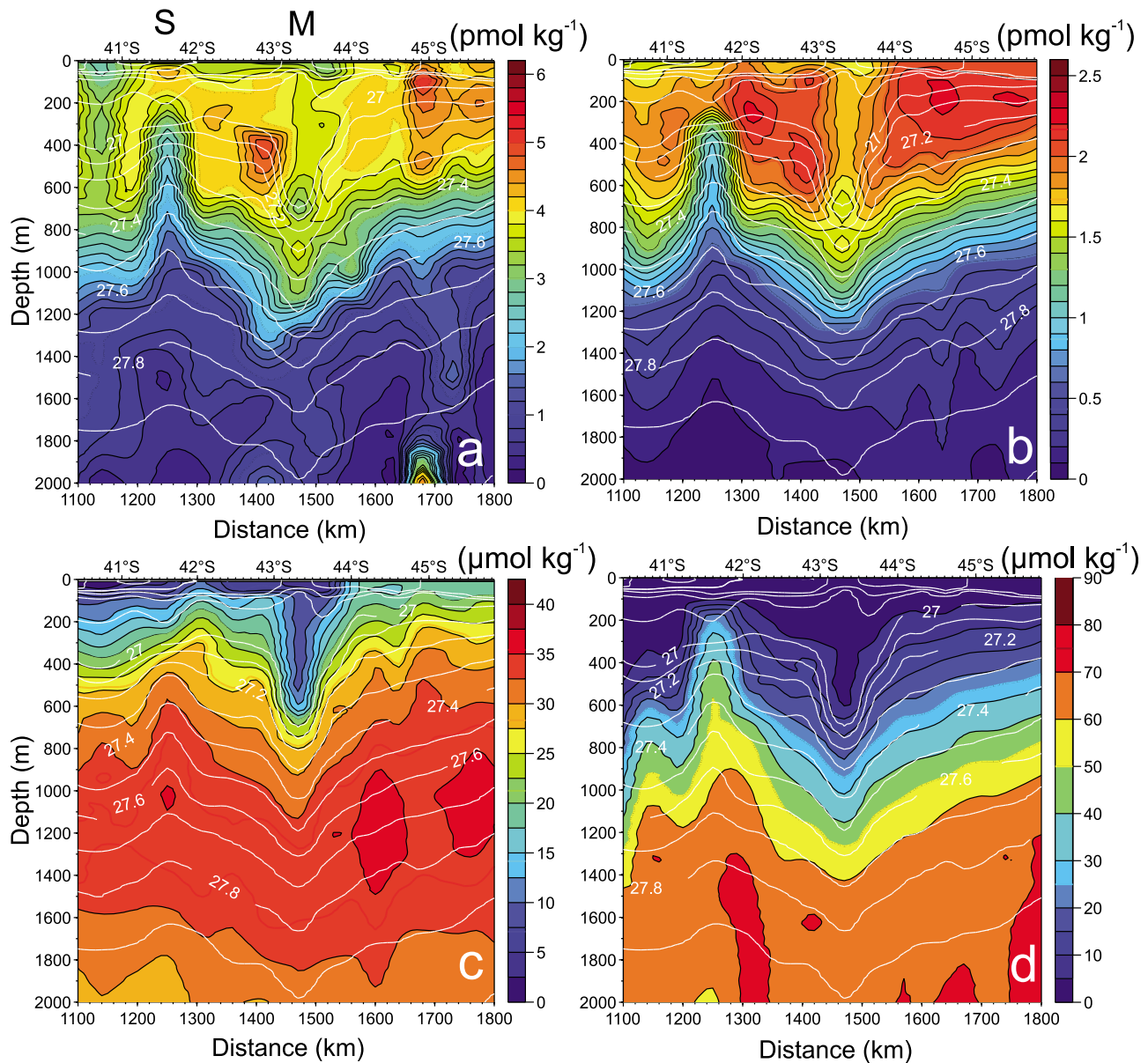


Figure 6. Vertical distributions of (a) CFC11, (b) CFC12, (c) nitrates, and (d) silicates across eddies M and S. Superimposed are the neutral density isopycnals.

which was observed 4 degrees of latitude farther north in March 1995. Eddy E3 described by *Gladyshev et al.* [2008], also sampled farther north during the 2004 GoodHope cruise, was slightly warmer, with homogeneous core temperatures of 12.5°C. Although all three eddies of Table 1 have similar high core oxygen values around 260 $\mu\text{mol kg}^{-1}$, the homogeneous core of eddy M is not as distinguishable in vertical sections of oxygen (Figure 5d) as its two counterparts (and as in temperature and salinity sections, Figures 5a and 5b). The reason for this lies in the surrounding oxygenated subantarctic waters. Eddies R1 and E3 of Table 1, being surrounded by less oxygenated subtropical water ($\sim 220 \mu\text{mol kg}^{-1}$), appeared as well-defined positive anomalies in their vertical oxygen distributions [Arhan *et al.*, 1999; Gladyshev *et al.*, 2008]. For eddy M, a contrast between the core and neighboring stations is better seen in the dissolved oxygen profiles themselves

(Figure 7b), the eddy side profiles being more irregular, and indicative of interleaving, than the central one. The oxygen signature of M is also more visible when using the oxygen saturation, instead of dissolved oxygen concentration. In Figure 8 showing the saturation at 300 m depth at all BGH stations, the core station of M stands out with a 0.98 value, well above neighboring rates around 0.85, and similar to the values computed for R1 and E3 (Table 1). Such oxygen saturations, and the thick homogeneous layer are indications of convection and ventilation of the eddy during the previous winter.

[14] The along-track vertical distributions of CFC-11 and CFC-12 (Figures 6a and 6b) also exhibit the water homogenisation at 100–600 m in eddy M, and pronounced low anomalies at the core stations, relative to values at the surrounding stations. The nitrate and silicate signatures of eddy M (Figures 6c and 6d) are characterized by low core

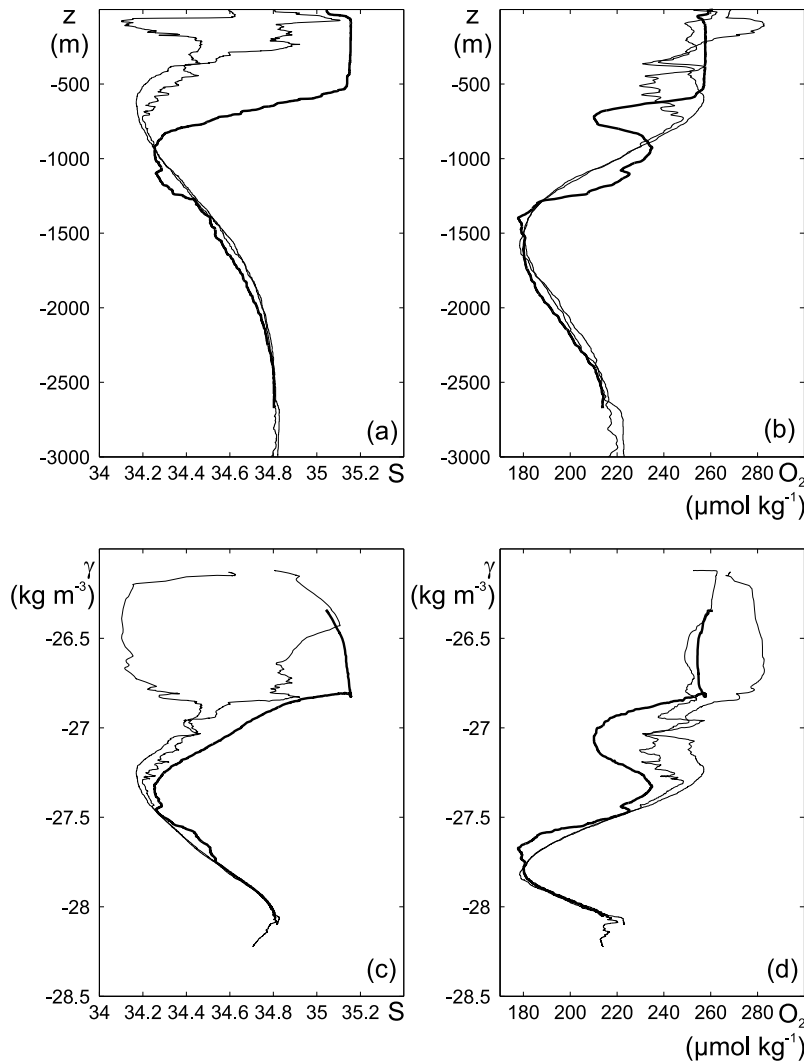


Figure 7. Property-property plots of station 47 in the core of eddy M and its adjacent stations: (a) salinity vertical profile, (b) dissolved oxygen vertical profile, (c) neutral density (γ)-salinity and (d) neutral density-dissolved oxygen diagrams.

values also indicative of winter convection. In the sharp pycnocline underlying the convected layer (Figure 5c), the core of eddy M is marked by low anomalies of dissolved oxygen, CFC-11, and CFC-12 concentrations at $\gamma \sim 27.1$ (700–800 m depth; Figures 5d, 6a, and 6b). The high salinities of the eddy homogeneous layer (>35.0), and the relative low oxygen ($\sim 225 \mu\text{mol kg}^{-1}$) and CFC concentrations at $\gamma = 27.1 \text{ kg m}^{-3}$ reflect an eddy origin at subtropical latitudes, the only domain where such values are found at similar densities (Figures 2a and 2b). These properties most certainly make this eddy an Agulhas ring, as was the case for the similar structures mentioned above (Table 1). Still deeper in the core of M, the salinity minimum of the Antarctic Intermediate Water (AAIW) is 34.25, also slightly above the ~ 34.2 values of the neighboring stations. *Gordon et al.* [1992] observed that two AAIW varieties exist in this region, namely, AAIW recently formed in the Atlantic sector (characterized by salinity minima lower than 34.3), and older AAIW from the Indian Ocean sector conveyed

south of Africa by the Agulhas Current (with salinity minima higher than 34.3). Although the AAIW salinity minimum in M bears the signature of the Atlantic sector, its high anomaly relative to the neighboring stations is also indicative of an Indian Ocean influence, and of an eddy origin in the Agulhas Current system.

[15] The above water property considerations on the origin of eddy M are best illustrated in the along-track distributions of salinity and dissolved oxygen plotted with neutral density as the vertical coordinate (Figures 9a and 9b). On Figures 9a and 9b the upper boundary provides the surface density and, slightly shifted (by 0.03 kg m^{-3}), the pluses show the densities at the base of the surface mixed layer. Most ACC fronts can be detected in Figure 9 from steeper slopes of this upper limit. The STF stands out particularly at $\sim 38^\circ\text{S}$ and also, though less pronounced, its southern expression at $\sim 42^\circ\text{S}$, and the Polar Front at $\sim 50^\circ\text{S}$. The SAF, on the other hand, is not marked by any increased slope, and even corresponds to a plateau at 44°S – 45°S , in

Table 1. Properties of the Homogeneous Cores of Eddy M and of Two Other Agulhas Rings With Convected Cores Described in Previous Studies

	θ ($^{\circ}\text{C}$)	S	γ (σ_{θ}) (kg m^{-3})	O_2 ($\mu\text{mol kg}^{-1}$)	O_2/O_2 Saturation	Latitude	Longitude	Source
Eddy M	11.8	35.15	26.82(26.75)	257.7	0.98	43 $^{\circ}$ 20'S	8 $^{\circ}$ 14'E	this study
Ring R1	11.6	35.08	(26.72)	263	0.99	39 $^{\circ}$ 30'S	11 $^{\circ}$ E	Arhan et al. [1999]
Eddy E3	12.5	35.2	26.75	255	0.98	39 $^{\circ}$ 12'S	11 $^{\circ}$ 21'E	Gladyshev et al. [2008]

accordance with Rintoul and Trull [2001] (and Gladyshev et al. [2008], along the GoodHope line), who pointed out the near-surface compensating effects of temperature and salinity on density across the SAF.

[16] The homogeneous core of M being represented by one point on such plots, is hardly visible. Its overlying pycnocline, on the other hand, appears as salty and moderately oxygenated relative to the neighboring stations. These contrasts most certainly reflect northward entrainment of fresher and oxygenated SAF water around the anticyclone. Deeper, the above mentioned oxygen minimum at $\gamma = 27.1 \text{ kg m}^{-3}$ appears as the southernmost manifestation of low oxygen values at densities 27.0–27.1 kg m^{-3} . Farther north this vertical oxygen minimum forms a continuous southward pointing tongue which emanates at the continental slope and protrudes well into the SAZ to $\sim 41^{\circ}\text{S}$. Given the intense mesoscale activity of the region, it is unlikely that this low oxygen tongue at $\gamma = 27.1 \text{ kg m}^{-3}$ is associated with a large scale flow. Very likely, it results from eddies akin to M penetrating the SAZ and losing a part of their intermediate, poorly oxygenated layer there.

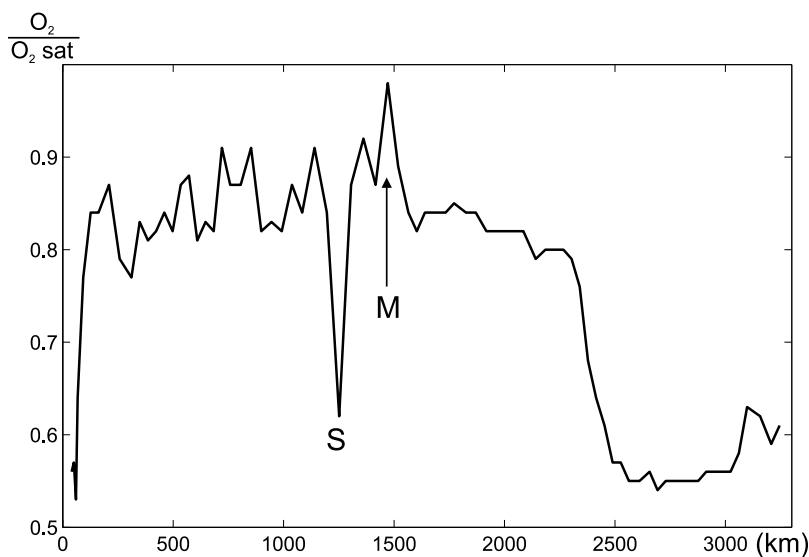
[17] The AAIW layer is centered on $\gamma = 27.35 \text{ kg m}^{-3}$ (Figure 9a), apparently also subject to mesoscale influences. Eddy M penetrates the upper part of this layer vertically at a short distance north of its subduction latitude. The AAIW salinity minimum at the eddy center ($S \sim 34.25$), although reflecting a dominant South Atlantic origin, is higher than at the stations next to the eddy core on its northern side, where values lower than 34.2 are observed. Such values being characteristic of the region south of the SAF indicate that,

also at these depths ($\sim 700 \text{ m}$), M is advecting northward (and helping to subduct) AAIW from the Polar Frontal Zone south of the SAF, into the SAZ.

3.2. History of Eddy M

[18] The trajectory of eddy M (Figure 10a) was determined using the same method as employed by Dencausse et al. [2010] (itself drawn from Doglioli et al. [2007]) to track Agulhas rings. Basically, it rests on wavelet analyses of the weekly SSH anomaly fields, a technique which provides the central positions and contours of eddies. If a structure is observed at a given date, a similar anomalous SSH pattern observed on the following week, which has its center within the contour of the former, is assumed to represent the same eddy. Repeating the process until no anomalous SSH pattern is found within the preceding contour provides the eddy trajectory. Having thus determined the eddy trajectory, the time series of its translation velocity could be obtained, and is represented in Figure 10b. The following description of the eddy history relies on Figures 10a and 10b, and on individual SSH maps at the referred dates, not shown here.

[19] Eddy M could be tracked back to 20 May 2007, when an Agulhas ring detached from the Agulhas Current retroflexion at $\sim 40^{\circ}\text{S}$ – 18°E , just east of the northeastern end of the Agulhas Ridge (location 1 in Figure 10). As frequently occurs [Dencausse et al., 2010], the Agulhas ring was rapidly (June 2007) split in two parts by the topography, eddy M being the southern part. Eddy M moved rapidly southwestward, and was further divided under the apparent stirring effect of neighboring cyclones. These two splitting

**Figure 8.** Dissolved oxygen saturations at 300 dbar along the track of the BGH line. The locations of eddies M and S are indicated.

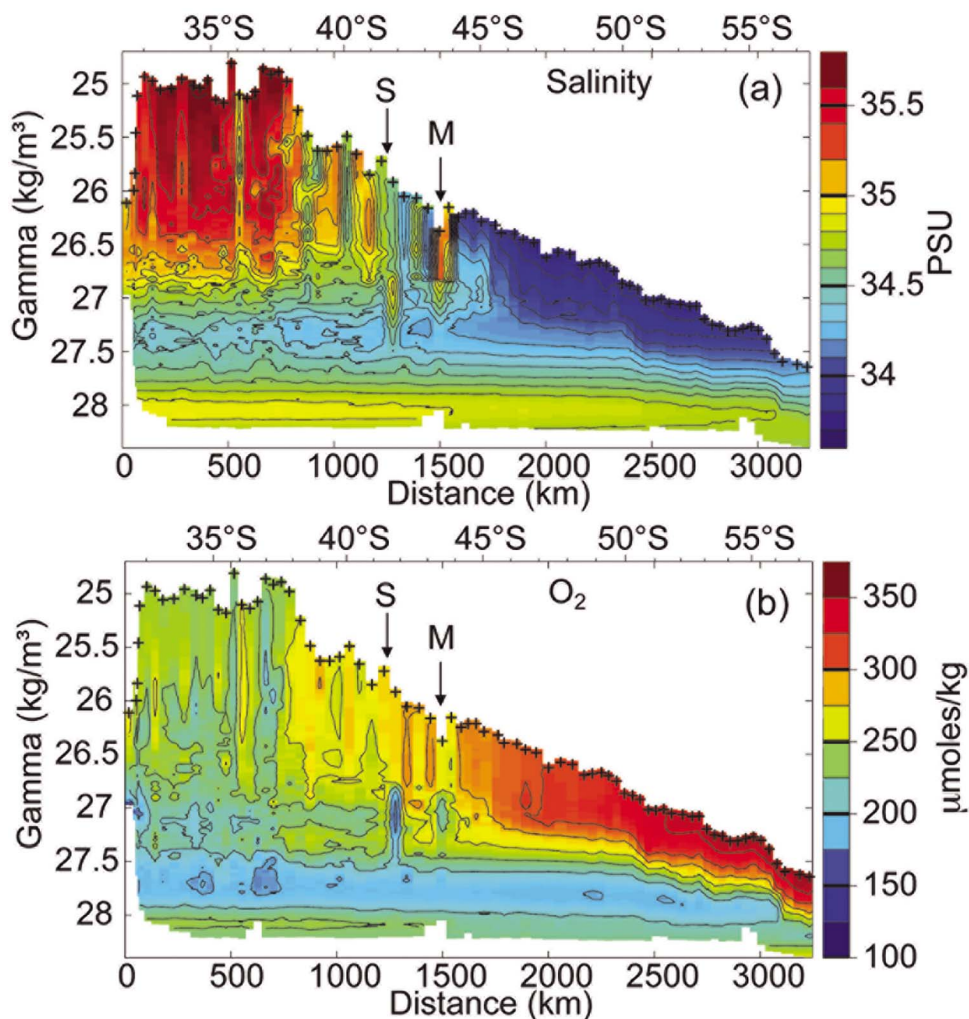


Figure 9. Vertical distributions of (a) salinity and (b) dissolved oxygen along the BGH line, represented with neutral density (γ) as the vertical coordinate.

events are certainly a major cause of the small radius of M (~ 70 km) as compared with usual values of 150–200 km (illustrated by the newly shed ring at 39°S–14°E in Figure 10a). On 25 July the eddy reached its first southern extreme position (location 2, 43°15′S–13°14′E) where it stayed for 2–3 weeks before resuming motion in a northward direction. This southernmost position for eddy M, and change of course, coincided with the eddy encounter with a northward meander of the SAF. The new (northward) part of the trajectory involved a very slow movement. Apparently, the eddy was blocked by the Agulhas Ridge, which was crossed only on 19 December 2007 (location 3, 41°36′S–11°34′E). Afterwards, a faster anticyclonic displacement led the eddy back over the bathymetry on 20 February 2008, where it was sampled during the BGH cruise (location 4, 43°19′S–8°14′E). At that period, it was slowly moving eastward, an indication of its entrainment by the neighboring SAF. Eddy M stalled a long time over the ridge, which it only left in mid-May 2008 toward the northwest. The surface signature of the eddy was lost in mid-August 2008 at 40°26′S–4°47′E, close to the STF where it most likely subducted below lighter water.

[20] Overall, eddy M could be tracked 15 months, and was 9.5 months old when it was observed during BGH. It belongs to what *Dencausse et al.* [2010] called the Agulhas ring southern family. Those eddies, after formation at the Agulhas Current retroflection, enter the region to the southeast of the Agulhas Ridge. Putting the emphasis on rings likely subject to significant property alterations before entering the South Atlantic, *Dencausse* [2009] paid a particular attention to those rings from the southern family which spend more than 4 months south of the Agulhas Ridge. A total of 14 such rings were detected in the SSH maps from the period October 1992 to January 2007 (Table 2), whose trajectories are drawn in Figure 11a. Their number amounts to about 50% of the whole southern family, the other half either dissipating in the SAZ without crossing the ridge, re-integrating the Agulhas Current retroflection or the Agulhas Return Current, or crossing the ridge rapidly close to its northeastern end. In order to assess the representativeness of eddy M, we present here the outlines of these 14 ring behaviors as inferred from their SSH tracking. About half of them formed from the subdivision of a

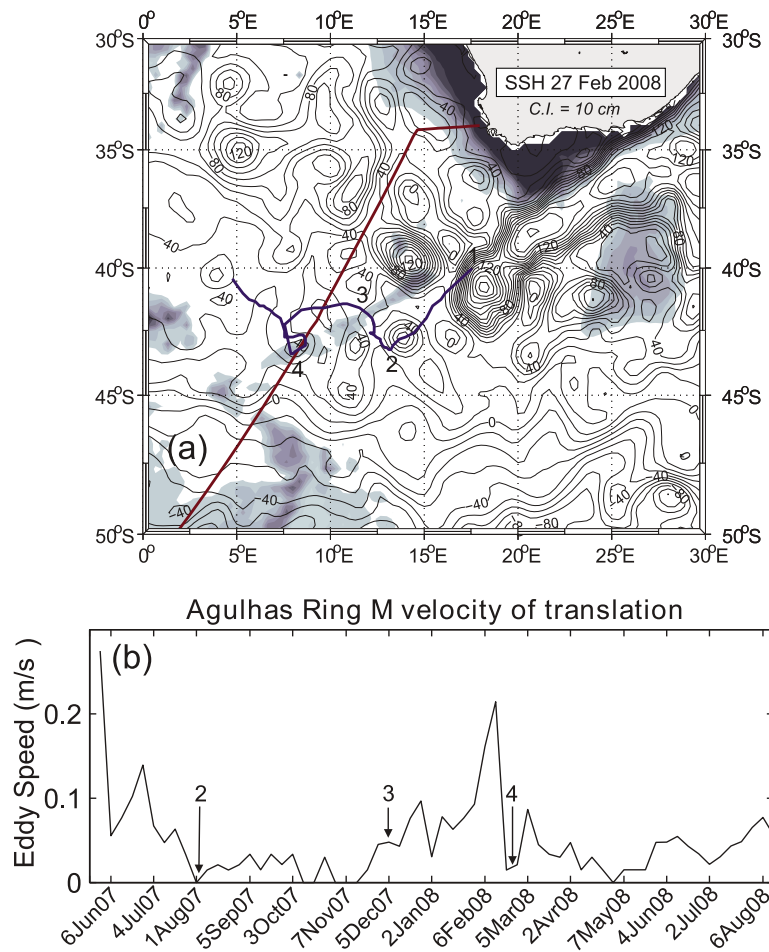


Figure 10. (a) Trajectory of eddy M, with the AVISO SSH map when observed during the BGH cruise. (b) Translation velocity of eddy M as function of time. Numbers 1, 2, 3, 4 refer to remarkable events described in the text.

newly spawned Agulhas ring at the northeastern end of the Agulhas Ridge. The other ones detached from the Agulhas Current Retroflexion itself, in situations when it protruded westward in a more southern position than usual. The initial

southward displacements of these eddies in the SAZ were rapid, and were only stopped when the eddies hit the SAF, which appears as an impassable barrier for these structures. The westward component of the eddy displacements is

Table 2. List of 14 Agulhas Rings Which Spent More Than 4 Months South of the Agulhas Ridge and Eventually Crossed It in the Northwestward Direction, During the Period October 1992 to January 2007^a

Eddy	Begin	End	Tracking Duration (weeks)	Time South of Agulhas Ridge (weeks)	Time South of Agulhas Ridge and Autumn/Winter (weeks)	Southernmost Latitude
32c	22 Jul 1998	27 Jan 1999	28	10	10	42°56'S
20	31 Jan 1996	13 Nov 1996	42	36	26	43°10'S
72a (E3)	17 Dec 2003	5 Jan 2005	54	36	27	43°30'S
83e	13 Jul 2005	25 Oct 2006	69	38	12	44°32'S
17a	2 Aug 1995	6 Mar 1996	30	14	6	42°26'S
98a (R1)	23 Mar 1994	22 Mar 1995	51	25	25	43°49'S
106a	22 Jul 1998	14 Jul 1999	50	30	9	43°00'S
60b	5 Jun 2002	27 Nov 2002	26	26	16	43°54'S
121	6 Oct 2004	2 Feb 2005	18	17	0	42°16'S
21	7 Feb 1996	26 Jun 1996	21	5	0	42°06'S
54g	22 Aug 2001	13 Nov 2002	65	32	7	42°36'S
133sd	1 Oct 1997	21 Jan 1998	17	17	0	43°25'S
129s	15 Jan 2003	19 Nov 2003	45	42	27	44°41'S
44_s	5 Apr 2000	9 Aug 2000	19	19	19	42°31'S
Average			38	24	13	43°12'S

^aFrom Dencausse [2009].

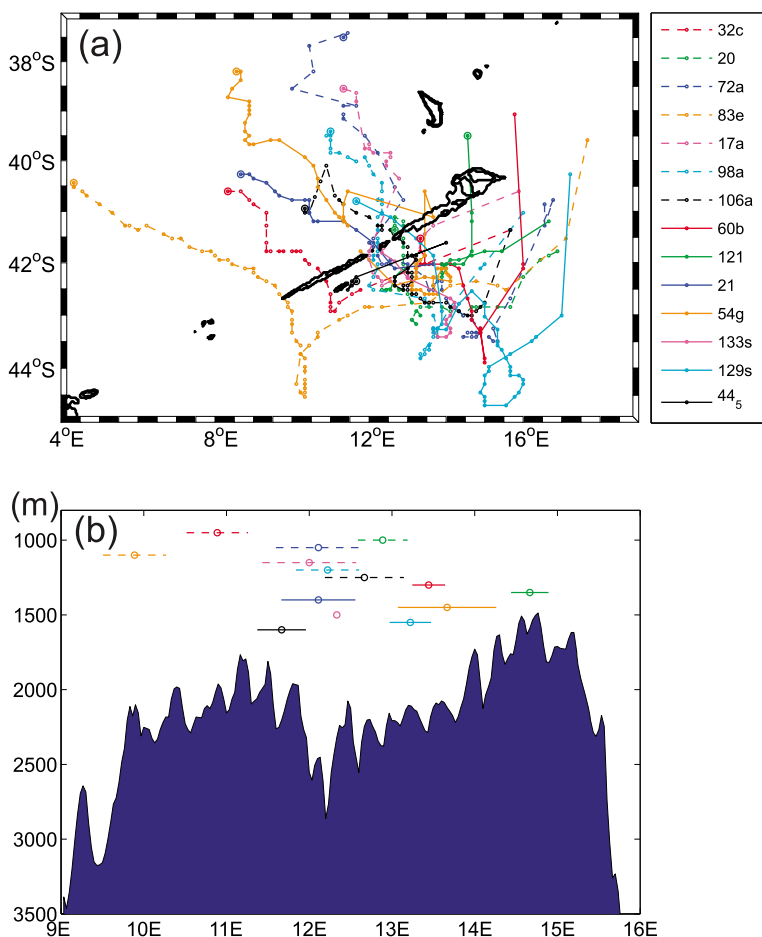


Figure 11. (a) AVISO-inferred trajectories of the 14 Agulhas rings listed in Table 2, which spent more than 4 months south of the Agulhas Ridge and eventually crossed it in the northwestward direction, in the period October 1992 to January 2007. (b) Crestline of the Agulhas Ridge as function of longitude, showing the locations where the rings of Table 2 crossed the ridge.

always slowed down when approaching the front, and even sometimes reverses into an eastward motion, causing a loop in the trajectories of several eddies (Figure 11a). While the first encounter of eddy M with the SAF does not exhibit any such loop (location 2 in Figure 10a), the second encounter does (location 4).

[21] After interacting with the SAF, the eddies generally move northwestward as did M, also with a lower velocity likely influenced by the vicinity of the Agulhas Ridge. Crossing of the Agulhas Ridge generally occurs at 12°E–13°E (Figure 11b), where a 2000–2500 m deep passage exists. Eddy M itself crossed the ridge at 11°34'E. Most trajectories could not be traced very far beyond the Agulhas Ridge. The longest ones terminate at 37°S–38°S, the very latitude range of the STF, where the eddies might be either dissipated or subducted [Herbette *et al.*, 2004]. Several of them had their trajectories interrupted as they merged with another anticyclone. This is another way of subducting, for, as they align with another (warmer) structure, the cooled eddies are capped by its lighter core. The disappearance of the eddy surface signatures is therefore not necessarily associated with their total dissipation. Observation of Agulhas rings with sub-

ducted (subsurface) homogeneous cores in the Cape Basin has been reported by McDonagh and Heywood [1999], Garzoli *et al.* [1999] and Arhan *et al.* [1999]. The erosion of the eddies of Figure 11, as measured from the decay of their SSH anomalies, was generally intense during the first stage of their lives, suggesting that it results from the modification of their core properties, rather than from interaction with the SAF, or crossing of the Agulhas Ridge.

[22] The core alterations may be significant, as Agulhas ring core temperatures initially around 17°C [e.g., Gordon *et al.*, 1987; van Aken *et al.*, 2003] may decrease to less than 12°C (as in M). They likely result from a combination of heat loss to the atmosphere and mixing with the surrounding subantarctic water [Arhan *et al.*, 1999]. A model study by Donners *et al.* [2004] illustrates how convection in the eddy core generates a shallow thermohaline circulation between the core and outer domain, which could enhance the lateral exchanges. The low temperatures of eddies M, R1, and E3 of Table 1 should be related to the fact that they all spent a whole autumn and winter period south of 42°S. Table 2 shows that, while on average the eddies spent about three months in autumn/winter south of the Agulhas

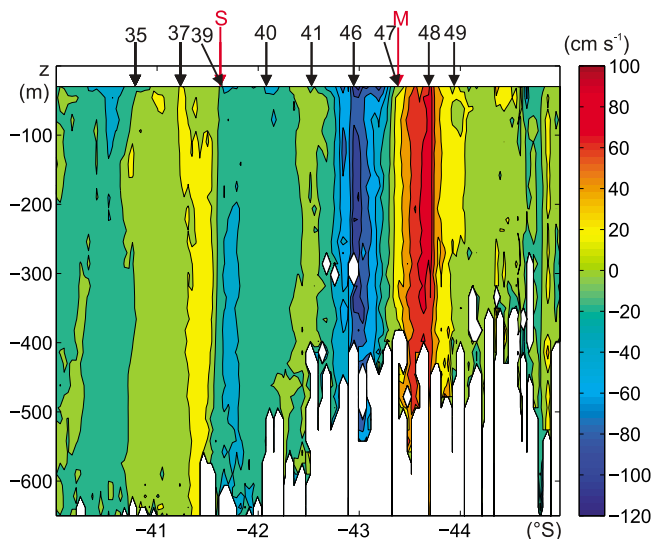


Figure 12. VM-ADCP velocity component perpendicular to the BGH section, across eddies M and S. Arrows give the locations of the full-depth hydrographic and L-ADCP stations.

Ridge, 4 of them, including R1 and E3, spent more than 6 months south of the ridge. The averaged southernmost latitude reached by the cooled Agulhas rings is $43^{\circ}12'S$, about the latitude reached by eddy M on its two southern excursions ($43^{\circ}15'S$ and $43^{\circ}20'S$). This latitude varies significantly, however (from $\sim 42^{\circ}S$ to $\sim 44^{\circ}40'S$), depending on whether the eddies collide with the SAF at developed northern, or southern, meanders.

[23] Except for the fact that eddy M encountered the SAF twice, this structure appears rather typical of the eddy family represented in Figure 11. The eventful lives of these eddies are remarkable. They often stem from the subdivision of an Agulhas ring, interact with the SAF, experience intense air-sea interaction, blocking by the Agulhas Ridge and, after eventually crossing it, often subduct on re-entering the subtropical domain they emanated from.

3.3. Eddy M Kinematics and Water Trapping

[24] Velocities in eddy M were measured during the BGH cruise using the VM-ADCP, the L-ADCP installed on the water sampling rosette frame, and can be inferred from geostrophy. Figure 12, showing the vertical distribution of the velocity component perpendicular to the GoodHope line at latitudes where eddies S and M were observed, also gives the locations of the hydrographic stations relative to the two structures. It so happened that station 47 was very close to the center of eddy M, and stations 46 and 48, located respectively at 55 km and 47 km from station 47, were only slightly on the outer side of the eddy lateral velocity maxima. Using the 5 km averaged VM-ADCP velocities, the azimuthal velocity maxima of eddy M can be located at ~ 45 km from the eddy center. Because the eddy is adjacent to the SAF in the south, inferring its outer radius on this side is difficult. On the northern side, a sharp velocity gradient (Figure 4) locates the outer radius at ~ 70 km. Vertically the velocities were highest at 190 m depth, with speeds of 1.2 m s^{-1} westward, and 0.98 m s^{-1} eastward. The geostrophic

velocities computed relative to 2500 dbar for station pairs 46–47 and 47–48 (Figure 13a) suggest that rotational velocities are detectable as deep as ~ 2000 m. The geostrophic velocity maxima, around 0.45 m s^{-1} in both directions are, as expected from the station locations near the eddy center and velocity maxima, about half those inferred from the VM-ADCP. The eddy rotational volume transport, computed from geostrophy, was found equal to 28 Sv.

[25] The L-ADCP profiles at stations 46 and 48 (Figure 14), close to the positions of the lateral velocity maxima, as expected show westward (eastward) highest velocities 1 m s^{-1} (0.8 m s^{-1}), only slightly lower than the 1.2 m s^{-1} (0.98 m s^{-1}) neighboring maxima. Figure 14 also confirms the ~ 2000 m thickness of the rotational motion, a value comparable to the depth of the Agulhas Ridge at $11^{\circ}34'E$ where eddy M first crossed this ridge, and necessarily left its deeper part behind. When observed during its second encounter with the Agulhas Ridge, eddy M was located above a ~ 2700 m culminating peak (Figure 4) and was therefore underlaid by a few hundreds of meters of non-rotating water. This corroborates our previous assumption that its southward motion was not stopped by the Agulhas Ridge, but by the SAF. Note that Figure 14 reveals a striking difference in the deep velocities at stations 46 and 48. At station 46, located above the northern flank of the Agulhas Ridge, the velocities nearly vanish at depths greater than ~ 2000 m. On the other hand, at station 48 located south of the ridge they increase downward at this depth, then keep values of $0.2\text{--}0.35 \text{ m s}^{-1}$ to the vicinity of the bottom at ~ 4500 m. These velocity observations recall a similar eastward flow, likely associated with the SAF, present in a schematic of the near-bottom circulation in that region, by Gladyshev *et al.* [2008]. A passage in the Agulhas Ridge, located slightly upstream at $\sim 6^{\circ}E$ (Figure 4) explains its presence against the southern flank of the ridge in the BGH data.

[26] Flierl [1981] demonstrated that water can be trapped in an eddy when its azimuthal speed exceeds its drift speed. First considering eddy M on 28 February 2008 when observed during BGH, its translation speed was about 0.03 m s^{-1} (Figure 10b), implying deep water trapping. Assuming, as observed from the VM-ADCP measurements at 0–400 m (Figure 13a), that the maximum azimuthal speed is twice the geostrophic velocity, a trapping depth around 2000 m is inferred at that time. The eddy translation velocity, however, varied significantly since the structure was formed (Figure 10b). During the two periods of southwestward motion (parts 1–2 and 3–4 in Figure 10a) the eddy moved at speeds of around 0.1 m s^{-1} with weekly peaks at $0.2\text{--}0.3 \text{ m s}^{-1}$. The eddy azimuthal velocities themselves likely decreased since it was formed. For a first approximation of trapping depths in M, we here assume that the eddy always had the maximum velocity profile estimated at its observation date. This is a likely conservative hypothesis producing underestimates of the trapping depths. This assumption leads to trapping depths of about 900 m, 1150 m, and 1500 m for drift velocities of 0.3 m s^{-1} , 0.2 m s^{-1} , and 0.1 m s^{-1} , respectively. With these values, and given the 0.3 m s^{-1} eddy drift velocity shortly after its formation, we can expect trapping of water from the formation region down to ~ 900 m. Given the $\sim 0.2 \text{ m s}^{-1}$ drift speed in February 2008 shortly before the observation date, we may also expect trapping of water from

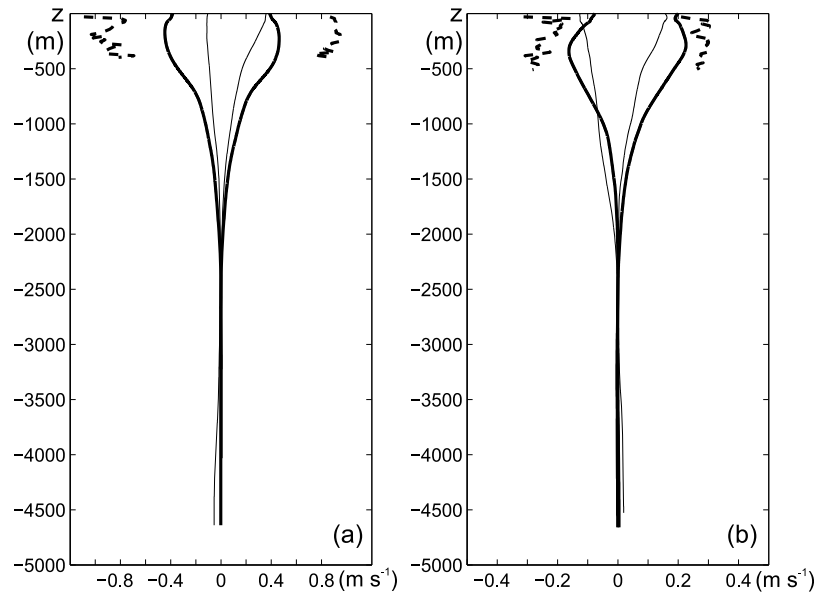


Figure 13. (a) Continuous lines indicate top-to-bottom geostrophic velocities referenced to 2500 dbar of station pairs 46–47, 47–48 (bold lines), 41–46 and 48–49 (thin lines) in eddy M. See Figure 12 for the station positions along the BGH cruise track. Dashed lines indicate profiles of lateral maxima of VM-ADCP velocities perpendicular to the cruise track. (b) Same as Figure 13a but for station pairs 37–39, 39–40 (bold), 35–37, 40–41 (thin) in eddy S.

the northern part of the SAZ between ~ 900 m and ~ 1150 m, and just local water below.

[27] Looking for confirmation of these inferences in water properties, we show in Figure 15 the along-track distributions of potential temperature, salinity and dissolved oxygen on four isopycnals: $\gamma = 27.1 \text{ kg m}^{-3}$ which is central to the low

oxygen anomaly at 700 m–850 m in M, $\gamma = 27.35 \text{ kg m}^{-3}$ which marks the AAIW core layer at ~ 1000 m in M, and $\gamma = 27.5 \text{ kg m}^{-3}$ (27.7 kg m^{-3}) at depth ~ 1200 m (~ 1450 m) in eddy M. Property extrema indicative of water trapping in the eddy exist at $\gamma = 27.1 \text{ kg m}^{-3}$, $\gamma = 27.35 \text{ kg m}^{-3}$, and $\gamma = 27.7 \text{ kg m}^{-3}$, not at greater densities, suggesting some

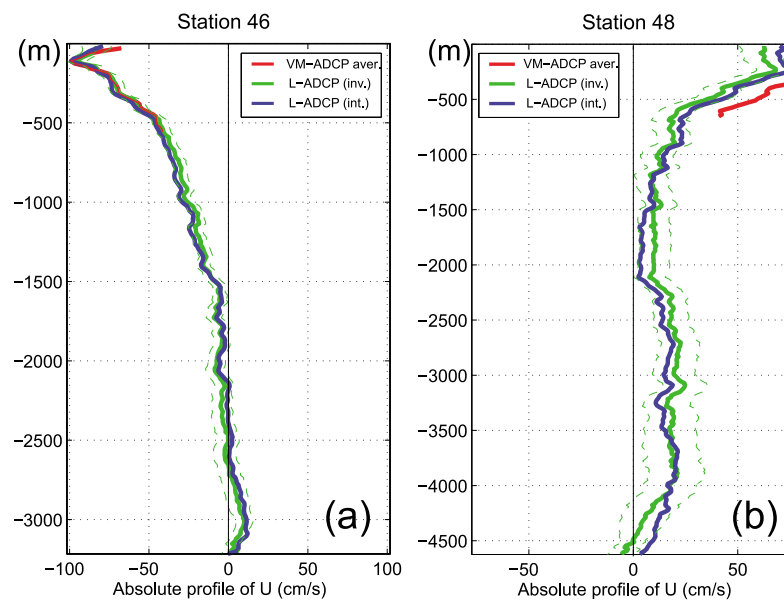


Figure 14. Top-to-bottom L-ADCP velocity profiles (zonal components) at stations 46 and 48 close to the locations of highest swirl velocities of eddy M along the BGH cruise track (see the stations locations in Figure 12). The green lines show the velocities computed using the inversion method [Visbeck, 2002], and the blue lines were obtained using the integration method [Gouriou and Kermabon, 1997]. Also shown (red) are the VM-ADCP measurements.

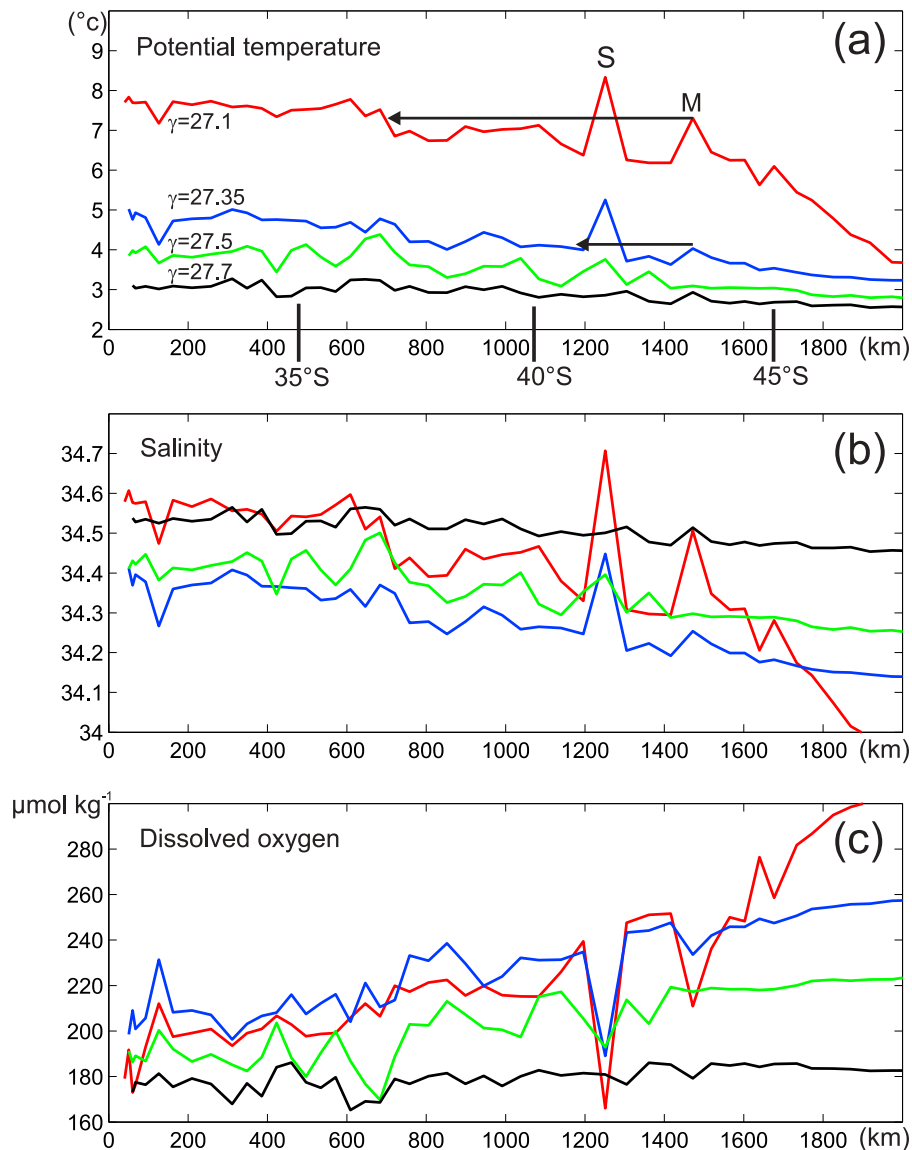


Figure 15. Distributions of (a) potential temperature, (b) salinity, and (c) dissolved oxygen on isopycnals $\gamma = 27.1 \text{ kg m}^{-3}$ (red), $\gamma = 27.35 \text{ kg m}^{-3}$ (blue), $\gamma = 27.5 \text{ kg m}^{-3}$ (green) and $\gamma = 27.7 \text{ kg m}^{-3}$ (black), along the track of the BGH cruise. The black horizontal arrows in Figure 15a illustrate how the origin of the water trapped in an eddy (here M) is inferred, for each isopycnal.

trapping of non local water down to $\sim 1500 \text{ m}$. The brief 0.2 m s^{-1} peak of drift velocity in early February 2008, therefore, apparently did not totally separate the eddy from its deeper-than-1200 m part. The only indication of its possible effect is the absence of property anomalies at 27.5 kg m^{-3} in Figure 15. Between the surface mixed layer and $\sim 600 \text{ m}$ in eddy M, the homogeneous water draws its high temperature and salinity from the eddy formation region, with subsequent modifications resulting from surface cooling and associated lateral exchanges. Below the homogeneous layer, the $\gamma = 27.1 \text{ kg m}^{-3}$ curves in Figures 15a–15c show that the 600–850 m oxygen minimum layer also originates in the eddy formation area. The eddy properties at this density are, indeed, only found north of 37°S , close to where the STF criteria were met along the BGH line. Still deeper, the weaker

property anomalies associated with eddy M at $\gamma = 27.35 \text{ kg m}^{-3}$ and $\gamma = 27.7 \text{ kg m}^{-3}$ are observed at $39^\circ 30'\text{S}$ – 41°S , just north of eddy S, in the northern part of the SAZ. Information on water trapping in eddy M gained from water properties therefore corroborates the inferences drawn from the kinematics above 1200 m. At 1200–2000 m, recent trapping is inferred from water properties, not from the kinematics. An ARGO profiler launched during BGH in the core of eddy M and drifting at 1000 m, itself suggests only a loose trapping at and below 1000 m. Its first temperature and salinity profiles, realized two days after launching at the core station of M, reproduced those of that station. However, the subsequent ones (10 days later and $\sim 100 \text{ km}$ from the launching point) showed no trace of the homogeneous layer, and the next ones (20 days later) had well-recognizable SAF character-

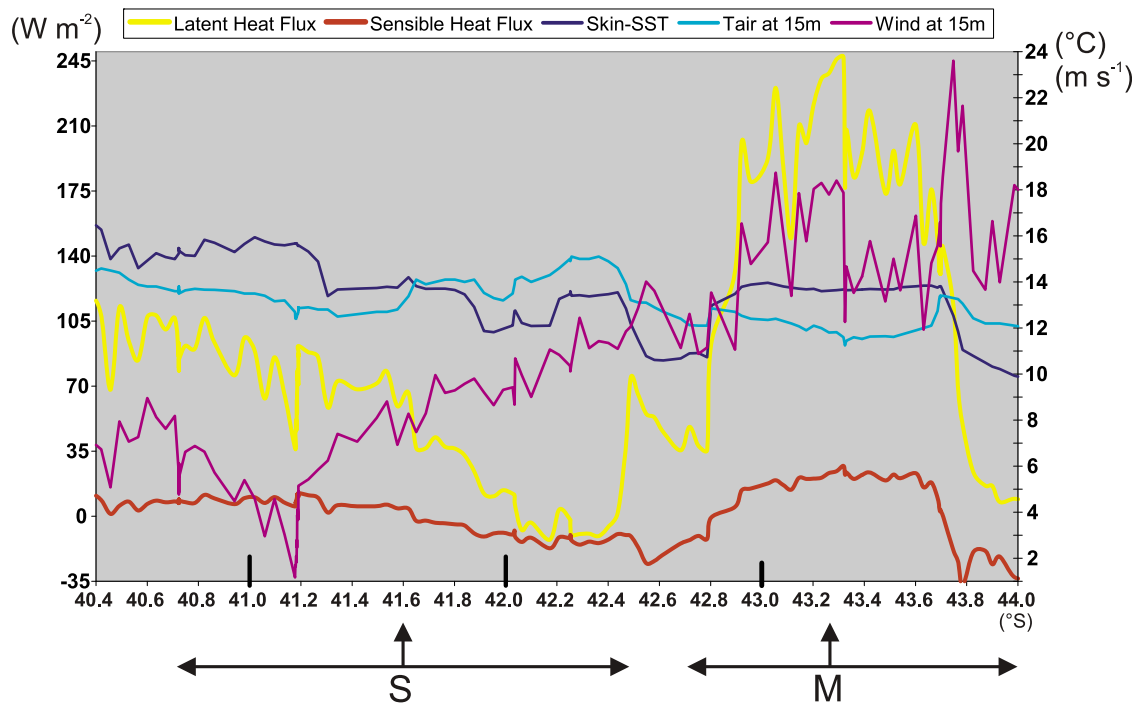


Figure 16. Air-sea exchange parameters along the BGH cruise track, in the region where eddies M and S were sampled: Latent heat flux (yellow), sensible heat flux (brown), skin sea surface temperature (black), air temperature (blue) and wind (purple) at 15 m. fluxes are positive when released from the ocean to the atmosphere. Arrows show the centers of eddies M and S, and their width defined as the latitude spans with rotational anticyclonic (for M) and cyclonic (for S) velocities are observed. Note that the graduations of the vertical axis at the right-hand side are common to the temperature and wind speed curves.

istics. This rapid expulsion of the profiler from eddy M might have been caused by the $\sim 0.1 \text{ m s}^{-1}$ maximum of eddy drift speed on 5 March 2008 (Figure 10b), combined with float descents to 2000 m before each profile.

3.4. Air-Sea Fluxes Over Eddy M

[28] Measuring surface heat fluxes over an Agulhas eddy centered at $\sim 42^\circ\text{S}$ - 20°E in June–July 1993; *Rouault and Lutjeharms* [2000] found that the structure was a substantial source of heat for the atmosphere, as a result of latent heat fluxes of 500 W m^{-2} , and sensible heat fluxes of 350 W m^{-2} . The eddy had somewhat the same origins as eddy M, but was likely younger, and sampled during the opposite season. It had a surface temperature up to $\sim 17^\circ\text{C}$ and a 250 m-thick mixed layer, whereas eddy M has surface temperatures slightly below 14°C , and a $\sim 50 \text{ m}$ summer mixed layer itself separated from the underlying $\sim 12^\circ\text{C}$ homogeneous core by a seasonal thermocline. We here present the surface heat flux computations over eddy M, thus allowing for a comparison with the *Rouault and Lutjeharms* [2000] eddy, and with the cyclonic eddy S (section 4). The surface turbulent fluxes of momentum, sensible and latent heat fluxes (hereafter SHF and LHF, respectively), were computed using the COARE bulk air-sea flux algorithm [Fairall et al., 2003] applied to the atmospheric measurements performed on board.

[29] The mean in situ Bowen ratio (between sensible and latent heat fluxes) along the summertime BGH cruise (0.041) indicates that a major part of the available energy at the ocean surface is passed to the atmosphere through evaporative processes. The evaporative fraction (0.96 over the whole cruise) is then appropriate for representing the relative contributions of the turbulent energy fluxes to the energy budget. During that summer, the LHF was mainly positive (not shown), indicating that along the cruise track the ocean mainly lost energy through evaporative turbulent processes, which are highly dependent on wind velocity.

[30] The sea surface skin temperature curve (Figure 16) reveals a well-defined high anomaly between 42.9°S (28°February) and 43.8°S (29°February), exactly above the location of eddy M. At these latitudes the air-sea temperature gradient is inverted, as compared to outside the eddy, and induces a positive SHF of 15 W m^{-2} on average (reaching up to 23.6 W m^{-2}) from the ocean to the atmosphere. In the same latitude interval, the LHF also presents a high average value of 180 W m^{-2} (reaching up to 247 W m^{-2}), and strongly contrasts with those outside the eddy.

[31] The ocean heat content between the surface and 100 m (not shown) revealed a positive energy anomaly of $6 \cdot 10^5 \text{ kJ/m}^2$ within eddy M, allowing a long-term and powerful release of energy as long as the structure remained south enough of the STF. The ocean isotherms within the

top 60 m revealed a warm anomaly within the eddy core (whose surface imprint is visible in Figure 16), even though a pronounced seasonal thermocline separated the summer surface mixed layer from the $\sim 12^\circ\text{C}$ homogeneous layer below. Although such thermoclines sometimes blur the surface expressions of underlying mesoscale anomalies, this was not the case for eddy M, a likely consequence of a tight surface water trapping. Provided that the eddy was not intersected too far from its center, its surface temperature imprint in Figure 16 suggests a surface trapping radius of 65 km, very close to the radius (70 km) inferred above from the rotational velocities of Figure 4. The sharp outer cut-off of these velocities, visible on the northern side of the structure, explains the near-coincidence of the two radius estimates.

[32] The wind magnitude (purple in Figure 16) exhibits an abrupt increase above the northern side of eddy M, which might have reflected a wind increase associated with the sea surface temperature anomaly of the structure [Small *et al.*, 2008]. This high wind episode, apparent at 42.6°S – 43.4°S , and the other one at the southern border of the eddy (43.7°S – 43.8°S), however, are related to the atmospheric synoptic eastward flux rather than to local eddy effects. Indeed, two low pressure systems crossed the cruise track flowing eastward during that period, the first one south of eddy M causing the first above mentioned wind increase, and the second one with a center closer to the structure producing the second wind peak. Such an interpretation was corroborated by an examination of the rotation of the wind direction, and the pressure variations, during the events.

[33] It was expected that the 9.5 month old eddy M, which was sampled during summer, would not be associated with as high heat fluxes to the atmosphere as the younger Agulhas ring sampled during winter by Rouault and Lutjeharms [2000]. The 200 W m^{-2} accumulated LHF and SHF computed for eddy M during a period of averaged wind speed $\sim 15\text{ m s}^{-1}$, is nevertheless quite significant. Such a summer value is partly due to the atmospheric environment of the structure, but also to the eddy capacity, to keep an important energy reserve in its uppermost tens of meters, despite the previous cooling of its upper core and the presence of a seasonal thermocline.

4. Cyclone S

4.1. Core Properties and Origin of Eddy S

[34] This description of the core properties of eddy S rests on the same diagrams as used for eddy M (Figures 2, 5, and 6), and on Figure 17 showing the salinity and oxygen profiles and the density–salinity and density–oxygen curves at the eddy core station 39 and at the neighboring stations 37 and 40. The two latter stations sampled the eddy rotational velocities (Figure 12), but were outside its hydrographic core.

[35] The upper 200 m of eddy S present water properties which are somewhere between those of the subtropical and subantarctic domains, as illustrated by values of 10.97°C and 34.56 psu at 100 m, which fall in the temperature and salinity ranges defining the STF of Orsi *et al.* [1995]. Between 200 m and 400 m, eddy S is characterized by vertical maxima in potential temperature (10.28°C at 260 m and $\gamma = 26.85\text{ kg m}^{-3}$), salinity (34.845 at 265 m and $\gamma = 26.89\text{ kg m}^{-3}$) and by pronounced oxygen minimum

($165.5\text{ }\mu\text{mol kg}^{-1}$ at 335 m and $\gamma = 27.07\text{ kg m}^{-3}$) and CFC concentration minima. These extrema coincide with a maximum of the Brunt–Väisälä frequency (Figure 5c) at the transition between an overlying depression and underlying uplift of isopycnals. Still deeper, at 400–900 m in the AAIW layer, the interior of eddy S (minimum salinity of 34.370 at 760 m and $\gamma = 27.52\text{ kg m}^{-3}$) is saltier than the outside. In addition, though the eddy is marked by a vertical oxygen maximum ($198\text{ }\mu\text{mol kg}^{-1}$), it remains less oxygenated than the surrounding waters. In Figures 17c and 17d, the AAIW salinity and oxygen vertical extrema at $\gamma = 26.52\text{ kg m}^{-3}$ (900 m) also mark the deepest point where the eddy core profiles differ from the neighboring ones. The vertical transition at this density is abrupt, suggesting that the non-local water of eddy S had just overlaid the local water at the date of observation. Like the oxygen signature of the eddy (Figure 5d), the CFC and nutrient structures (Figure 6) appear as upward pointing tongues of low values (for the CFCs) and high values (for the nutrients). As the tongue-shaped patterns generally cross the density contours, these eddy anomalies are more than just an isopycnal uplift of properties, and reflect trapping and transport of distant water by the eddy.

[36] The above description of the core anomalies of eddy S reveals a subtropical influence at all levels above $\sim 900\text{ m}$ ($\gamma = 27.5\text{ kg m}^{-3}$). In Figures 9a and 17c, a major characteristic of the eddy is a high salinity anomaly at $26.75\text{ kg m}^{-3} < \gamma < 27.5\text{ kg m}^{-3}$, whose origin can only be north of the STF. The AAIW salinity minimum of 34.37, well above the 34.3 limit separating the old Indian Ocean and recent Atlantic Ocean varieties in that region, itself undoubtedly points to a subtropical origin. The best marker of the eddy origin, however, is its low oxygen concentration ($165.5\text{ }\mu\text{mol kg}^{-1}$) at $\gamma = 27.07\text{ kg m}^{-3}$, which is only found at similar densities (and combined with similar temperatures and salinities) at the South African continental shelf break (Figures 2b and 9b). This narrow core of low oxygen concentrations at the continental slope, here observed west of Cape Town at $33^\circ 58'\text{S}$, shows a minimum of $150\text{ }\mu\text{mol kg}^{-1}$ at 290 m and $\gamma = 27.04\text{ kg m}^{-3}$, comparable to a previous nearby ($34^\circ 18'\text{S}$) observation of $146\text{ }\mu\text{mol kg}^{-1}$ at 250 m by Mercier *et al.* [2003]. In both cases, VM-ADCP measurements showed that the oxygen-depleted water near the continental slope is associated with a poleward alongshore undercurrent at 150–300 m. Farther east, Chapman *et al.* [1987] also observed low oxygen water ($< 180\text{ }\mu\text{mol kg}^{-1}$) at 50–200 m along the continental slope, which was associated with the Agulhas Current, and separating from the coast with it. Although it is uncertain whether both features are connected, water with oxygen as low as $160\text{ }\mu\text{mol kg}^{-1}$ at 50–300 m appears as characteristic of the alongslope flows around South Africa. The closeness of the oxygen minimum and associated density in eddy S ($165.5\text{ }\mu\text{mol kg}^{-1}$, $\gamma = 27.07\text{ kg m}^{-3}$) to those of the near-slope water at $33^\circ 58'\text{S}$ is remarkable. The southward influence of the coastal low oxygen water appears in Figures 2b and 9b through patches of low oxygen ($< 200\text{ }\mu\text{mol kg}^{-1}$) at $\gamma = 27.1\text{ kg m}^{-3}$ north of the STF and, as mentioned above, through a large southward tongue with values below $225\text{ }\mu\text{mol kg}^{-1}$ reaching to 41°S . The core of low oxygen observed at $\sim 700\text{ m}$ in eddy M also had this density ($\gamma = 27.05\text{ kg m}^{-3}$), yet showing higher concentrations ($210\text{ }\mu\text{mol kg}^{-1}$) indicative of

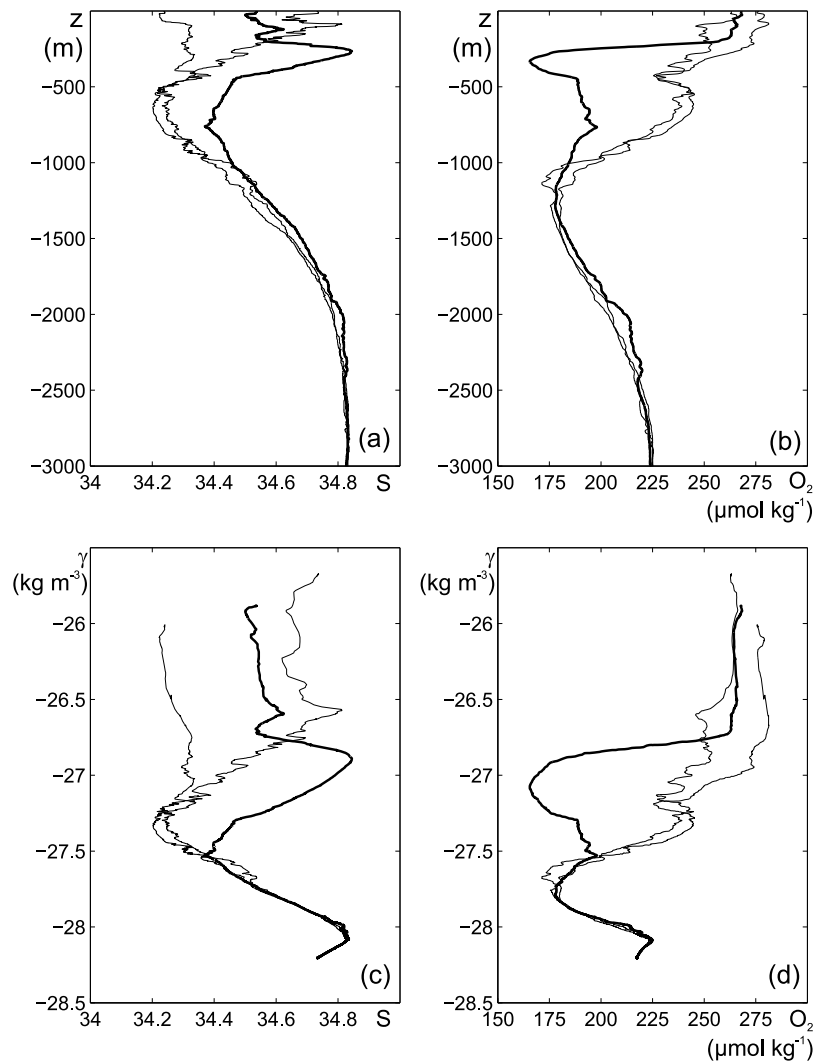


Figure 17. Property-property plots of station 39 in the core of eddy S and its neighboring stations: (a) salinity vertical profile, (b) dissolved oxygen vertical profile, (c) neutral density (γ)-salinity and (d) neutral density (γ)-dissolved oxygen diagrams.

dilution, did not imply an origin right at the continental slope for that eddy.

4.2. History of Eddy S

[37] Because eddy S was smaller in size and less intense than eddy M, its backtracking using the method of *Dencausse et al.* [2010] proved more difficult. Backtracking could only be performed over two months, to mid-December 2007. Before this date, we had to track eddy S visually, an admittedly less rigorous method which, however, appeared unambiguous, and should provide a correct trajectory, insofar as the SSH maps themselves are correct. Tracking by the wavelet method did not work, either, after the date of the eddy observation during BGH. We also had to rely on visual tracking for that period, and on information from an ARGO profiler launched in S. For lack of a complete detailed trajectory, we show in Figure 18 six weekly SSH maps at dates of outstanding events in the life of eddy S. The eddy trajectory, determined as just described, is shown in Figure 18e.

[38] The formation of eddy S was around 10 October 2007 (Figure 18a), when a cyclone was present at 39°S-20°E south of the Agulhas Bank, separating the Agulhas Current retroflexion from an Agulhas ring that detached from it about two weeks before. On that date, the SSH low anomaly of eddy S extends southward beyond 40°S into the SAZ, suggesting that the structure might be formed of subantarctic water entrained northward by the eastern part of the newly spawned ring [*Lutjeharms and van Ballegooyen*, 1988]. The eddy, however, seems also connected to another cyclonic structure present west of the Agulhas Bank, a connection which was still more apparent in the previous SSH map. This frequently observed cyclone west of the Agulhas Bank was named the “lee eddy” by *Penven et al.* [2001]. It is fed from the east by cyclonic vorticity cores propagating southwestward along the continental slope [*Lutjeharms et al.*, 2003]. The formation process of eddy S shows that the distinction between subantarctic cyclones (stemming from the SAZ) and Agulhas cyclones (originating in the lee eddy) might not be clear-cut. Furthermore, we noted above that very low oxygen

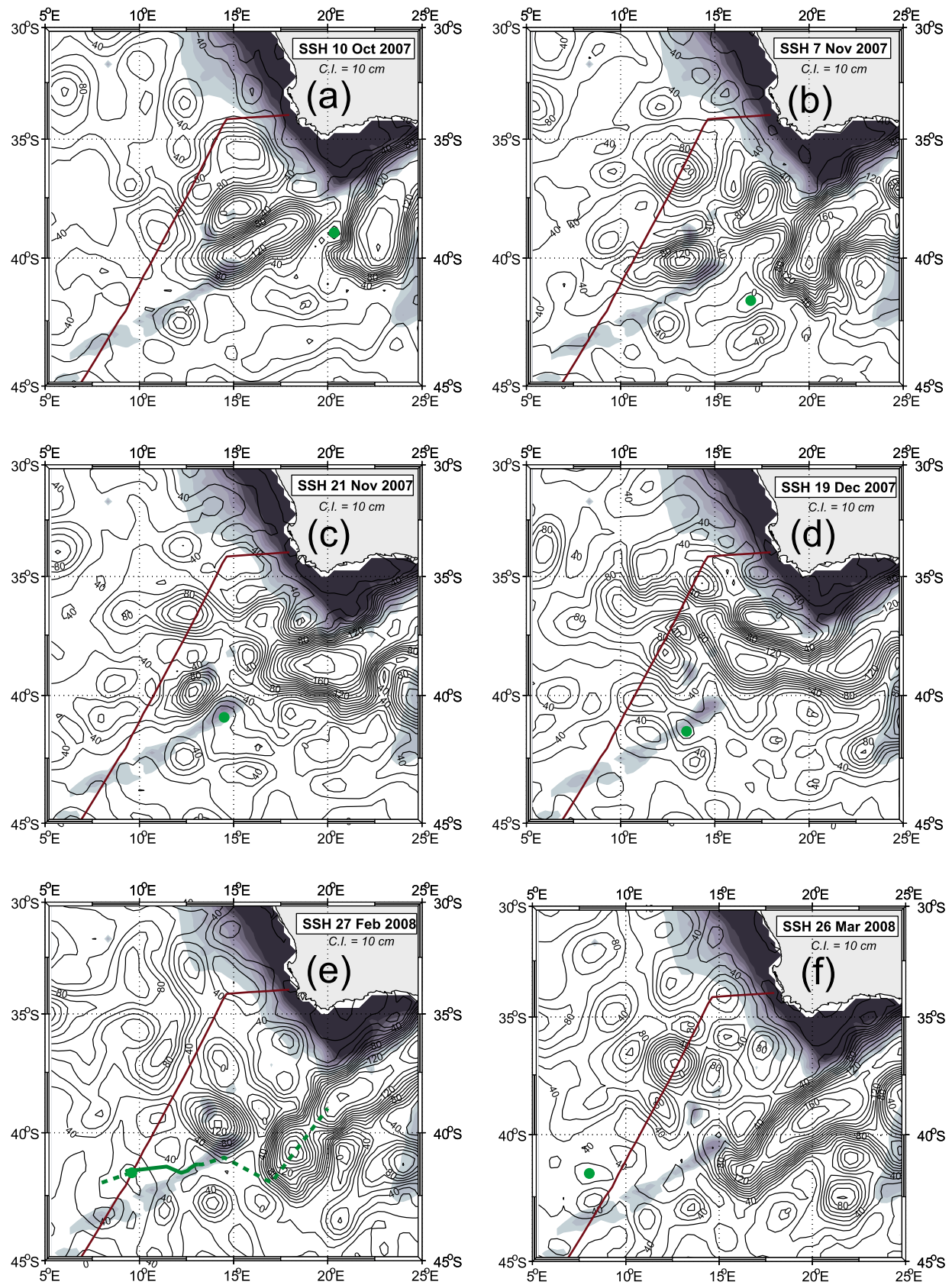


Figure 18. AVISO Sea Surface Height maps illustrating the history of eddy S (see text). The green dots show the positions of the eddy. Also shown in Figure 18e is the eddy trajectory determined partly as by *Dencausse et al.* [2010] (continuous), and partly visually (dashed).

concentrations ($<160 \mu\text{mol kg}^{-1}$) at $\gamma = 27.1 \text{ kg m}^{-3}$ as observed in eddy S might be more representative of the poleward undercurrent at the Atlantic continental shelf break, than of the Agulhas Current, making this undercurrent possibly a third contributing source for eddy S. Whatever its dominant origin (Agulhas Current, Atlantic poleward undercurrent, subantarctic domain), the observation that eddy S was adjacent to the continental slope in early October 2007 would alone explain its marking by along-slope water characteristics, including low oxygen.

[39] On 7 November 2007 (Figure 18b), eddy S was at 42°S – 17°E , still close to the Agulhas Current retroflection, yet was stirred and being subdivided by the combined effects of the retroflecting current and nearby vortices. Eddy S, the southern part of the subdivision, moved away from the Agulhas Current retroflection, and, after another subdivision, found itself above the northeastern end of the Agulhas Ridge (41°S – $14^\circ30'\text{E}$) on 21 November 2007 (Figure 18c). After stalling three weeks over the bathymetry, the eddy moved southwestward, then crossed the ridge northwestward on 19 December 2007 (Figure 18d) at $41^\circ15'\text{S}$ – $13^\circ20'\text{E}$. At about this date eddy S became adjacent to eddy M, and it may be that entrainment of S by M helped the former cross the ridge. It is also from this date onward that S could be tracked by the wavelet method. On 27 February, when observed during BGH (Figure 18e), eddy S was northeast of eddy M, still adjacent to the bigger eddy and apparently coupled to it, as its anticyclonic drift suggests. The SSH signal of S was lost about one month later on 26 March 2008 near 42°S – 8°E (Figure 18f).

[40] An ARGO profiler launched in eddy S on 26 February 2008 suggests that the eddy lived still longer, to at least 18 June 2008 (Figure 19). The salinity profiles provided at 10 days intervals (not shown) indeed exhibited patterns characteristic of the eddy until that date, namely, a salinity maximum at 250–300 m and a salinity minimum in the AAIW higher than 34.3. As such properties were observed exclusively in eddy S in the SAZ during BGH (Figure 2a), they indicate that the profiler remained for about 3 months in the eddy. After 18 June 2008, the ARGO profiles changed abruptly, as best seen from the potential temperature–salinity diagrams of Figure 19b, indicating that the float left the vortex. The float trajectory until that date (Figure 19a) confirms the anticyclonic drift of eddy S around M, its last detected position being 41°S – 8°E .

[41] Overall, eddy S lived for at least 8 months, and was 4.5 months old when observed during BGH. This being significantly more than the average duration of 2–3 months for cyclones inferred by *Boebel et al.* [2003] from altimetric tracking, suggests a great variability in the life durations of these structures. The net southwestward translation velocity of eddy S was 0.06 m s^{-1} . This is somewhat higher than previous average velocities of 0.036 m s^{-1} , obtained from altimetry by *Boebel et al.* [2003] and 0.041 m s^{-1} obtained from subsurface floats by *Richardson* [2007], yet lower than the 0.096 m s^{-1} surface drifter estimate by the latter author. The route followed by eddy S is at the southern fringe of the ensembles of cyclone trajectories [*Boebel et al.*, 2003; *Morrow et al.*, 2004; *Richardson*, 2007] and, in that, are more typical of Agulhas cyclones than Cape Basin cyclones trajectories. *Richardson* [2007] mentioned cyclones which stalled near the Schmitt-Ott Seamount (see Figure 1) at the

eastern end of the Agulhas Ridge, and noted that several cyclones trajectories terminated near the ridge. Eddy S seems also illustrative of such topographic effects, as it experienced subdivision near the tip of the Agulhas Ridge, and the part of the subdivision further tracked under the name of eddy S itself stalled for 3 weeks over the bathymetry. Regarding water properties, *Boebel et al.* [2003] stressed that while doming isopycnals in cyclones of that region create a surface signal seemingly indicative of an intrusion of water from the SAZ, the true origin of these features can only be revealed by their intermediate depth properties. Eddy S is also illustrative of this point. As noted above, while its SSH signatures tend to connect the eddy to the SAZ when just formed, and to the SAF when observed during BGH, its subtropical origin is only revealed by the 200–900 m water properties.

4.3. Eddy S Kinematics and Water Trapping

[42] Figure 12 shows that the lateral maxima of swirl speeds in eddy S, unlike those of eddy M, fall in the middle of the hydrographic stations intervals. This is a less favorable configuration which did not allow us to get full depth estimates of the azimuthal velocities from the L-ADCP. We had to rely on the geostrophic and VM-ADCP velocities displayed in Figure 13b. A ratio of 1.5 between the maximum azimuthal velocity and the geostrophic velocity, estimated from the top 600 m where VM-ADCP measurements were available (Figure 13b), was assumed to hold downward to ~2000 m, where velocities vanish.

[43] From the VM-ADCP data, (Figures 4b and 12), the lateral velocity maxima are at ~15 km only from the eddy center, and the eddy radius, defined as the outer limit of cyclonic swirl velocities, is ~90 km. Vertically, the velocities show maxima of 0.3 m s^{-1} at depths of 290 m (on the northward side of the eddy) and 350 m (on the southward side). The eddy rotational volume transport was found equal to 17.3 Sv eastward and 14.4 Sv westward.

[44] The objective tracking of eddy S that could be performed between mid-December and 26 February revealed a weak drift velocity of 0.03 m s^{-1} the week before the observation. During the 3 preceding weeks, however, the drift speed was ~ 0.15 m s^{-1} westward, a high value likely associated with the anticyclonic entrainment of eddy S by eddy M. Referring to the water trapping criterion of *Flierl* [1981] and to the profile of maximum swirl velocity obtained by applying the ratio 1.5 to the geostrophic velocities, the trapping depth was found equal to ~1600 m at the time of observation, and ~880 m during the three preceding weeks. Estimating the drift speed of the eddy after its observation can only be done from the displacements of the ARGO profiler, which includes a swirl component in addition to the eddy drift itself. Averaging the profiler displacements over the 10 cycles of 10 days during which it stayed in the vortex (Figure 19b), an average drift velocity of 0.1 m s^{-1} was found, which corresponds to a trapping depth of ~1100 m. From the above, it is likely that the water trapped in eddy S (down to ~1600 m) at the date of its observation during BGH was non-local water above ~880 m, and local water below.

[45] The profiles and density–property curves in the core of S and at neighboring stations (Figure 17) fit in with these inferences. The salinity and oxygen core profiles of S (Figures 17a and 17b) differ significantly from those of the side stations above ~950 m, and are very similar to the latter

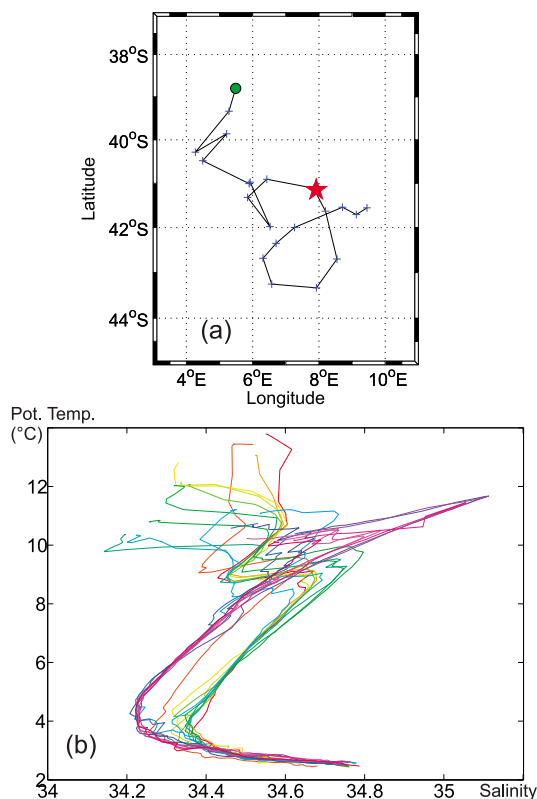


Figure 19. (a) Trajectory of ARGO profiler 1900864 during the period 29 February 2008 to 16 September 2008. The green circle marks the last position. (b) Potential temperature–Salinity diagrams of all profiles shown in Figure 19a, revealing an abrupt water mass modification on 18 June 2008 (star in Figure 19a), likely associated with the expulsion of the profiler from eddy S.

below. The γ -salinity and γ -oxygen curves (Figures 17c and 17d) exhibit the two vertical domains still more strikingly, with an abrupt transition at $\gamma = 27.6$ located at 900 m in the core of eddy S. This abrupt vertical transition is a sign that vertical mixing has not had time to operate since the non-local water of the eddy overlaid the local waters. It corroborates the conclusion drawn from the kinematics, that the high drift velocities of the preceding weeks split the eddy vertically at ~ 880 m. The fact that the ARGO profiler, which drifts at 1000 m, remained in the eddy for 3 months is compatible with the above estimate of a ~ 1100 m average trapping depth during that period. This is somewhat surprising, however, as temporary shallower trapping depths must have occurred during the 3 months, and the profiler sinks down to 2000 m every 10 days. A possible initial launching right at the eddy center, and the relatively large eddy radius (90 km) might be explanations for the observed trapping duration. Finally, the isopycnic property distributions along the cruise track (Figure 15) corroborate and bring more precision on the trapped water and its origin. The waters in eddy S at densities $\gamma = 27.1 \text{ kg m}^{-3}$ (~ 350 m depth in the eddy) and $\gamma = 27.35 \text{ kg m}^{-3}$ (510 m) evidently originate from the close vicinity of the continental slope where the eddy was formed. The water at $\gamma = 27.5 \text{ kg m}^{-3}$ (800 m) is subtropical water from north of $\sim 37^\circ\text{S}$, but not

from the eddy formation region. The absence of any signal related to eddy S at $\gamma = 27.7 \text{ kg m}^{-3}$ (~ 1100 m) confirms the presence of local water at such levels.

4.4. Air-Sea Fluxes Over Eddy S

[46] Eddy S, when intersected, was located under a flat low pressure that was widely spread from $20^\circ\text{S}/5^\circ\text{W}$ to south of the Agulhas retroflexion area. This flat low pressure was separating a deep perturbation centered at 55°S and moving eastward from a slow low pressure system located over the Agulhas retroflexion. This synoptic situation produced the lowest wind observed during the cruise (1.16 m.s^{-1} at 41.18°S ; Figure 16). This was an ideal atmospheric condition to investigate a warm eddy impact on the atmospheric boundary layer. Unfortunately, as mentioned above, eddy S was located just north of the southern STF branch, whose temperature gradient masked any sea surface temperature variation possibly related to the core of eddy S. As a consequence, the surface fluxes do not show any signal that might be related to this structure. The oceanic skin sea surface temperatures present higher values than the atmospheric temperature north of the STF, as expected. The warmer water there produces a positive SHF toward the atmosphere as well as a LHF. The fluxes then decrease steadily southward to beyond the STF, and collapse when the air-sea temperature gradient reverses at 41.65°S , inducing a negative SHF (energy transfer from the atmosphere to the ocean) and a LHF lower than 35 W.m^{-2} .

5. Conclusions

[47] The above analyses of eddies M and S illustrate the capacity of such structures to transfer subtropical properties to the SAZ. While some anticyclones eventually return to the subtropical domain, it is nevertheless expected that a partial release of their water and properties takes place in the SAZ. When observed, both eddies were found to trap subtropical water down to ~ 900 m, the water transported below this depth being either from the northern part of the SAZ, or just local water. Due to their contrasting vertical structures (bowl-shaped isopycnals in eddy M, doming isopycnals in eddy S), eddy S transports subtropical water of higher density (up to $\gamma = 27.5 \text{ kg m}^{-3}$, mostly Indian Ocean AAIW) than does eddy M (up to $\gamma = 27.25 \text{ kg m}^{-3}$, mostly South Indian Ocean Central Water modified by air-sea interaction).

[48] In addition to heat, the eddies convey other subtropical properties into the SAZ. One is salinity, particularly visible in the anticyclone cross section (Figure 5b) and, to a lesser extent, at $\gamma = 27.1 \text{ kg m}^{-3}$ in the cyclone. Salinity plays an important role in the vertical destabilization of the cores of the anticyclones under surface cooling conditions, and in their ensuing convection and saturation in atmospheric tracers [Olson *et al.*, 1992]. Other subtropical properties transported by these eddies are the low oxygen and CFC characteristic of the alongslope flows, and most certainly, though not sampled here, lithogenic tracers gained by the water during its contact with the continental slope. The low oxygen anomaly at $\gamma = 27.1 \text{ kg m}^{-3}$ appears as a particularly good tracer of those waters which were in contact with the continental slope. Low oxygen concentration was found in both eddies and the initial signal is found, more or less diluted, in the form of patches in the subtropical domain, and

as a continuous tongue in the SAZ. These observations point to the role of the eddies in contributing to the large scale property distributions in this region through a release of their core waters to the surroundings.

[49] There have been previous samplings of Agulhas rings that had experienced core water convection in the SAZ. With a core temperature around 12°C, eddy M ranges among the coldest of these structures, a consequence of its spending a whole winter in the SAZ. Despite this, and despite the sampling season, eddy M was still releasing $\sim 200 \text{ W m}^{-2}$ to the atmosphere when observed under $\sim 15 \text{ m s}^{-1}$ wind conditions. The swirl velocities $\sim 1 \text{ m s}^{-1}$ in this eddy are particularly high, given its age (9.5 months), and the fact that it crossed the Agulhas Ridge; *van Aken et al.* [2003] described a 2-month old Agulhas ring at 38°S, whose highest velocities, found at the sea surface, did not exceed those of M at $\sim 200 \text{ m}$. Obviously, the dynamical erosion of the eddy that would be expected from the cooling of its core was compensated by its moving into the cooler and denser environment of the SAZ. This sampling of a cooled Agulhas ring was also particular in that it occurred when M was adjacent to the SAF, and the cross sections of property distributions are indicative of SAF water being entrained northward (into the SAZ) by the vortex, at upper and intermediate levels. Such encounters of cooled Agulhas rings with the SAF, which regularly occur, might therefore be a process favoring transfer across this front. Part of this process may involve northward crossing of South Atlantic AAIW, and subduction of this water. These anticyclones then would not only favor a southward transport of subtropical properties, but also a northward transport of Polar Zone waters, into the SAZ.

[50] Subantarctic cyclones formed in the SAZ have long been known to exist in the subtropical domain. It was *Boebel et al.* [2003] who first brought to light the Agulhas and Cape Basin cyclones, and noted the unavailability of hydrographic data in which the origin of these new cyclone species near the continental slope would be recognized. Owing to its pronounced oxygen signature, eddy S appears as a characteristic example of such structures. It was observed far from its formation region ($\sim 1000 \text{ km}$) in a subantarctic environment strongly contrasting with its core waters. Its life duration estimate of ~ 8 months (relying on the ARGO profiler trajectory) is higher than the average tracking durations previously reported for cyclones. With highest swirl velocities of $\sim 0.3 \text{ m s}^{-1}$, its capacity to trap alongshore water down to $\sim 900 \text{ m}$, and to keep it unmodified for at least 4.5 months, is remarkable. Eddy S originated in the pool of cyclonic vorticity often present west of the Agulhas Bank and known as the lee eddy. *Lutjeharms et al.* [2003] described the part played by the lee eddy in the detachment of Agulhas rings from the Agulhas Current retroflection. *Dencausse et al.* [2010] underlined its influence on the westernmost positions reached by the retroflection, and its role in blocking the northwestward motion of some Agulhas rings. The capacity of the lee eddy to shed cyclonic mesoscale vortices southwestward was revealed by *Boebel et al.* [2003] and *Richardson* [2007]. This study provides an illustration of its properties being transported into, and influencing, the SAZ. The lee eddy, therefore, appears as a key feature of this important oceanographic

region, whose impact on the larger scale circulation should be better understood.

[51] **Acknowledgments.** This study is dedicated to the memory of Volfrango Rupolo (ENEA, Italy), a member of the Physical Oceanography group of the BGH cruise, who intended to participate to this analysis of the eddies sampled during the cruise. We are thankful to the Master, Pierre Courtès, the officers and crew of the R/V *Marion Dufresne*, for their precious help and cooperation, to Xavier Perrot for the preparation of the ADCP velocities, and to all other contributors to the numerous measurements used in the article. The IPY/BONUS-GoodHope and CLIVAR/GoodHope projects received support from the Institut National des Sciences de l'Univers (INSU), the CNRS, the Ifremer program "Circulation Océanique," the French Polar Institut Paul-Emile Victor (IPEV), the Agence Nationale de la Recherche (ANR), the Institut Universitaire Européen de la Mer (IUEM), and the University of Brest (UBO).

References

- Arhan, M., H. Mercier, and J. R. E. Lutjeharms (1999), The disparate evolution of three Agulhas rings in the South Atlantic Ocean, *J. Geophys. Res.*, *104*, 20,987–21,005, doi:10.1029/1998JC900047.
- Baker-Yeboah, S., D. A. Byrne, and D. R. Watts (2010a), Observations of mesoscale eddies in the South Atlantic Cape Basin: Baroclinic and deep barotropic eddy variability, *J. Geophys. Res.*, *115*, C12069, doi:10.1029/2010JC006236.
- Baker-Yeboah, S., G. R. Flierl, G. G. Sutyryn, and Y. Zhang (2010b), Transformation of an Agulhas eddy near the continental slope, *Ocean Sci.*, *6*, 143–159, doi:10.5194/os-6-143-2010.
- Belkin, I. M., and A. L. Gordon (1996), Southern Ocean fronts from the Greenwich meridian to Tasmania, *J. Geophys. Res.*, *101*, 3675–3696, doi:10.1029/95JC02750.
- Boebel, O., J. Lutjeharms, C. Schmid, W. Zenk, T. Rossby, and C. Barron (2003), The Cape Cauldron: A regime of turbulent inter-ocean exchange, *Deep Sea Res., Part II*, *50*, 57–86, doi:10.1016/S0967-0645(02)00379-X.
- Branellec, P., M. Arhan, and S. Speich (2010), Projet GoodHope: Campagne BONUS/GOODHOPE—Rapport de données CTD-O2, Ifremer internal report, *Rep. OPS/LPO/10-02*, 282 pp., Ifremer, Issy-les-Moulineaux, France. [Available at http://stockage.univ-brest.fr/~speich/BONUS_GoodHope/gh08-rapp-hydroSM.pdf.]
- Chapman, P., C. M. Duncombe Rae, and B. R. Allanson (1987), Nutrients, chlorophyll and oxygen relationships in the surface layers at the Agulhas Retroflection, *Deep-Sea Res.*, *34*, 1399–1416, doi:10.1016/0198-0149(87)90134-8.
- Dencausse, G. (2009), Echanges indo-atlantiques d'eau subtropicale en relation aux structures frontales et de méso-échelle: Utilisation de la série temporelle altimétrique de niveau de la mer, thèse de doctorat, 214 pp., Univ. de Bretagne Occidentale, Brest, France.
- Dencausse, G., M. Arhan, and S. Speich (2010), Routes of Agulhas rings in the southeastern Cape Basin, *Deep Sea Res., Part I*, *57*, 1406–1421, doi:10.1016/j.dsr.2010.07.008.
- Dencausse, G., M. Arhan, and S. Speich (2011), Is there a continuous Subtropical Front south of Africa?, *J. Geophys. Res.*, *116*, C02027, doi:10.1029/2010JC006587.
- Doglioli, A. M., B. Blanke, S. Speich, and G. Lapeyre (2007), Tracking coherent structures in a regional ocean model with wavelet analysis: Application to Cape Basin eddies, *J. Geophys. Res.*, *112*, C05043, doi:10.1029/2006JC003952.
- Donners, J., S. S. Drijfhout, and A. C. Coward (2004), Impact of cooling on the water mass exchange of Agulhas rings in a high resolution ocean model, *Geophys. Res. Lett.*, *31*, L16312, doi:10.1029/2004GL020644.
- Fairall, C. W., E. F. Bradley, J. E. Hare, A. A. Grachev, and J. B. Edson (2003), Bulk parameterization on air-sea fluxes: Updates and verification for the COARE algorithm, *J. Clim.*, *16*, 571–591, doi:10.1175/1520-0442(2003)016<0571:BPOASF>2.0.CO;2.
- Fine, R. A. (2011), Observations of CFCs and SF₆ as ocean tracers, *Annu. Rev. Mar. Sci.*, *3*, 173–195, doi:10.1146/annurev.marine.010908.163933.
- Fine, R. A., M. J. Warner, and R. F. Weiss (1988), Water mass modifications at the Agulhas Retroflection: Chlorofluoromethane studies, *Deep Sea Res.*, *35*, 311–332, doi:10.1016/0198-0149(88)90013-1.
- Flierl, G. R. (1981), Particle motions in large amplitude wave fields, *Geophys. Astrophys. Fluid Dyn.*, *18*, 39–74, doi:10.1080/03091928108208773.
- Garzoli, S. L., P. L. Richardson, C. M. Duncombe Rae, D. M. Fratantoni, G. J. Goni, and A. J. Roubicek (1999), Three Agulhas rings observed during the Benguela Current Experiment, *J. Geophys. Res.*, *104*, 20,971–20,985, doi:10.1029/1999JC900060.

- Gladyshev, S., M. Arhan, A. Sokov, and S. Speich (2008), A hydrographic section from South Africa to the southern limit of the Antarctic Circumpolar Current at the Greenwich meridian, *Deep Sea Res., Part I*, *55*, 1284–1303, doi:10.1016/j.dsr.2008.05.009.
- Gordon, A. L., J. R. E. Lutjeharms, and M. L. Gründlingh (1987), Stratification and circulation at the Agulhas retroflection, *Deep Sea Res.*, *34*, 565–599, doi:10.1016/0198-0149(87)90006-9.
- Gordon, A. L., R. F. Weiss, M. W. Smethie Jr., and M. J. Wamer (1992), Thermocline and intermediate water communication between the South Atlantic and Indian Oceans, *J. Geophys. Res.*, *97*, 7223–7240.
- Gouriou, Y., and C. Kermabon (1997), Traitement des données LADCP, *Doc. Sci. ORSTOM Cayenne O.P.21*, Off. de la Rech. Sci. et Tech. d'Outre-Mer, Paris.
- Herbette, S., Y. Morel, and M. Arhan (2004), Subduction of a surface vortex under an outcropping front, *J. Phys. Oceanogr.*, *34*, 1610–1627, doi:10.1175/1520-0485(2004)034<1610:SOASVU>2.0.CO;2.
- Izenic, Y., C. Kermabon, F. Gaillard and P. Lherminier (2005), Cascade 5.3: Logiciel de traitement et d'analyse des mesures ADCP de coque—Documentation utilisateur. Rapport technique, Ifremer, Issy-les-Moulineaux, France.
- Lutjeharms, J. R. E. (1988), Meridional heat transport across the Sub-Tropical Convergence by a warm eddy, *Nature*, *331*, 251–254, doi:10.1038/331251a0.
- Lutjeharms, J. R. E., and H. R. Valentine (1988), Eddies at the Subtropical Convergence south of Africa, *J. Phys. Oceanogr.*, *18*, 761–774, doi:10.1175/1520-0485(1988)018<0761:EATSCS>2.0.CO;2.
- Lutjeharms, J. R. E., and R. C. van Ballegooyen (1988), The retroflection of the Agulhas Current, *J. Phys. Oceanogr.*, *18*, 1570–1583, doi:10.1175/1520-0485(1988)018<1570:TROTAC>2.0.CO;2.
- Lutjeharms, J. R. E., O. Boebel, and H. T. Rossby (2003), Agulhas cyclones, *Deep Sea Res., Part II*, *50*, 13–34, doi:10.1016/S0967-0645(02)00378-8.
- McDonagh, E. L., and K. J. Heywood (1999), The origin of an anomalous ring in the southeast Atlantic, *J. Phys. Oceanogr.*, *29*, 2050–2064, doi:10.1175/1520-0485(1999)029<2050:TOOAAAR>2.0.CO;2.
- Mercier, H., M. Arhan, and J. R. E. Lutjeharms (2003), Upper-layer circulation in the eastern equatorial and South Atlantic ocean in January–March 1995, *Deep Sea Res., Part I*, *50*, 863–887, doi:10.1016/S0967-0637(03)00071-2.
- Morrow, R., F. Birol, D. Griffin, and J. Sudre (2004), Divergent pathways of cyclonic and anti-cyclonic ocean eddies, *Geophys. Res. Lett.*, *31*, L24311, doi:10.1029/2004GL020974.
- Olson, D. B., R. A. Fine, and A. L. Gordon (1992), Convective modifications of water masses in the Agulhas, *Deep Sea Res.*, *39*, S163–S181, doi:10.1016/S0198-0149(11)80010-5.
- Orsi, A. H., T. Whitworth III, and W. D. Nowlin (1995), On the meridional extent and fronts of the Antarctic Circumpolar Current, *Deep Sea Res. Part I*, *42*, 641–673, doi:10.1016/0967-0637(95)00021-W.
- Penven, P., J. R. E. Lutjeharms, P. Marchesiello, C. Roy, and S. J. Weeks (2001), Generation of cyclonic eddies by the Agulhas Current in the lee of the Agulhas Bank, *Geophys. Res. Lett.*, *28*, 1055–1058, doi:10.1029/2000GL011760.
- Richardson, P. L. (2007), Agulhas leakage into the Atlantic estimated with subsurface floats and surface drifters, *Deep Sea Res. Part I*, *54*, 1361–1389, doi:10.1016/j.dsr.2007.04.010.
- Rintoul, S. R., and T. W. Trull (2001), Seasonal evolution of the mixed layer in the Subantarctic Zone south of Australia, *J. Geophys. Res.*, *106*, 31,447–31,462, doi:10.1029/2000JC000329.
- Rouault, M., and J. R. E. Lutjeharms (2000), Air-sea exchange over an Agulhas eddy at the Subtropical Convergence, *Global Atmos. Ocean Syst.*, *7*, 125–150.
- Rubio, A., B. Blanke, S. Speich, N. Grima, and C. Roy (2009), Mesoscale eddy activity in the southern Benguela upwelling system from satellite altimetry and model data, *Prog. Oceanogr.*, *83*(1-4), 288–295, doi:10.1016/j.pocean.2009.07.029.
- Small, R. J., S. P. DeZoeke, S. P. Xie, L. O'Neill, H. Seo, Q. Song, P. Cornillon, M. Spall, and S. Minobe (2008), Air–sea interaction over ocean fronts and eddies, *Dyn. Atmos. Oceans*, *45*, 274–319, doi:10.1016/j.dynatmoce.2008.01.001.
- Speich, S., and F. Dehaies (2008), The MD166 BONUS-GOODHOPE cruise, LPO UMR 6523, CNRS-IFREMER-IRD-UBO, *Rep. OPS/LPO/08-06*, 245 pp., Ifremer, Issy-les-Moulineaux, France.
- Stramma, L., and R. G. Peterson (1990), The South Atlantic Current, *J. Phys. Oceanogr.*, *20*, 846–859, doi:10.1175/1520-0485(1990)020<0846:TSAC>2.0.CO;2.
- Swart, S., and S. Speich (2010), An altimetry-based gravest empirical mode south of Africa: 2. Dynamic nature of the Antarctic Circumpolar Current fronts, *J. Geophys. Res.*, *115*, C03003, doi:10.1029/2009JC005300.
- Swart, S., S. Speich, I. J. Ansorge, G. J. Goni, S. Gladyshev, and J. R. E. Lutjeharms (2008), Transport and variability of the Antarctic Circumpolar Current south of Africa, *J. Geophys. Res.*, *113*, C09014, doi:10.1029/2007JC004223.
- van Aken, H. M., A. K. van Veldhoven, C. Veth, W. P. M. de Ruijter, P. J. van Leeuwen, S. S. Drijfhout, C. P. Whittle, and M. Rouault (2003), Observation of a young Agulhas ring, Astrid, during MARE in March 2000, *Deep Sea Res., Part II*, *50*, 167–195, doi:10.1016/S0967-0645(02)00383-1.
- Visbeck, M. (2002), Deep velocity profiling using lowered acoustic Doppler current profilers: Bottom track and inverse solutions, *J. Atmos. Oceanic Technol.*, *19*(5), 794–807, doi:10.1175/1520-0426(2002)019<0794:DVPULA>2.0.CO;2.

M. Arhan and C. Messenger, Laboratoire de Physique des Océans, UMR6523, CNRS/Ifremer/IRD/UBO, Ifremer/Centre de Brest, BP 70, F-29280 Plouzané, France.

M. Boye, Laboratoire des Sciences de l'Environnement Marin, UMR6539, CNRS/IRD/UBO, IUEM, Technopole Brest Iroise, F-29280 Plouzané, France.

G. Dencausse, LEGOS/OMP, 14 Av. Edouard Belin, F-31400, Toulouse, France.

R. Fine, RSMAS/MAC, University of Miami, 4600 Rickenbacker Cswy., Miami, FL 33149-1098, USA.

S. Speich, Laboratoire de Physique des Océans, UMR6523, CNRS/Ifremer/IRD/UBO, UBO-UFR Sciences et Techniques, 6 Av. Le Gorgeu, CS 93837, F-29238 Brest CEDEX 3, France. (sabrina.speich@univ-brest.fr)